5-2017

What Are the Low-Q and Large-x Boundaries of Collinear QCD Factorization Theorems?

E. Moffat
Old Dominion University

W. Melnitchouk

T. C. Rogers
Old Dominion University

N. Sato

Original Publication Citation

Moffat, E., Melnitchouk, W., Rogers, T. C., & Sato, N. (2017). What are the low-Q and large-x boundaries of collinear QCD factorization theorems? *Physical Review D, 95*(9), 096008. doi:10.1103/PhysRevD.95.096008

What are the low-Q and large-x boundaries of collinear QCD factorization theorems?

E. Moffat,[1,*] W. Melnitchouk,[2,†] T. C. Rogers,[1,2,‡] and N. Sato[2,§]

[1]*Department of Physics, Old Dominion University, Norfolk, Virginia 23529, USA*
[2]*Jefferson Lab, 12000 Jefferson Avenue, Newport News, Virginia 23606, USA*

(Received 24 February 2017; published 26 May 2017)

Familiar factorized descriptions of classic QCD processes such as deeply inelastic scattering (DIS) apply in the limit of very large hard scales, much larger than nonperturbative mass scales and other nonperturbative physical properties like intrinsic transverse momentum. Since many interesting DIS studies occur at kinematic regions where the hard scale, $Q \sim 1$–2 GeV, is not very much greater than the hadron masses involved, and the Bjorken scaling variable $x_{\rm bj}$ is large, $x_{\rm bj} \gtrsim 0.5$, it is important to examine the boundaries of the most basic factorization assumptions and assess whether improved starting points are needed. Using an idealized field-theoretic model that contains most of the essential elements that a factorization derivation must confront, we retrace the steps of factorization approximations and compare with calculations that keep all kinematics exact. We examine the relative importance of such quantities as the target mass, light quark masses, and intrinsic parton transverse momentum, and argue that a careful accounting of parton virtuality is essential for treating power corrections to collinear factorization. We use our observations to motivate searches for new or enhanced factorization theorems specifically designed to deal with moderately low-Q and large-$x_{\rm bj}$ physics.

DOI: 10.1103/PhysRevD.95.096008

I. INTRODUCTION

Factorization theorems deal with the way interactions at different spacetime scales disentangle, for certain classes of scattering processes, in the asymptotically large limit of some physical energy [1]. They are especially important in QCD where asymptotic freedom enables calculations of short-distance partonic amplitudes using small-coupling perturbation theory. Many interesting applications of QCD factorization in hadronic physics are in regions where small-coupling techniques are likely to be useful, but where familiar kinematical approximations are perhaps questionable, and where the interplay between perturbative and nonperturbative physics becomes more intricate than at the very highest available energies.

Deeply inelastic scattering (DIS) of leptons from hadrons at moderately low momentum transfers Q is a prototypical example of this. Scales of $Q \sim 1$–2 GeV correspond to $\alpha_s/\pi \lesssim 0.1$, where α_s is the QCD running coupling, so it is reasonable to expect small-coupling methods to be applicable. Nevertheless, the success of those methods may require a careful account of effects beyond what is incorporated into the most straightforward and familiar applications of collinear QCD factorization.

Over the past three decades there has been significant progress in extracting quantitative information about the partonic structure of the nucleon from high-energy cross sections within the framework of collinear factorization. Indeed, a wealth of data from a wide range of high-energy processes, covering many orders of magnitude of the momentum transfer Q and the Bjorken scaling variable $x_{\rm bj}$, can be described in terms of universal sets of parton distribution functions (PDFs), both spin-averaged and spin-dependent—see Refs. [2–4] for recent reviews. The essential elements of the collinear factorization framework can be summarized as follows:

(1) Factorized formula. An observable, such as a structure function, F, is a convolution integral over a longitudinal parton momentum fraction, ξ, of a (hard) partonic coefficient function, $\hat{H}$, and a (soft) PDF, f,

$$F(x_{\rm bj}, Q) = \int_{x_{\rm bj}}^{1} \frac{{\rm d}\xi}{\xi} \hat{H}\left(\frac{x_{\rm bj}}{\xi}, \frac{\mu}{Q}\right) f(\xi, \mu) + O\left(\frac{m}{Q}\right), \tag{1}$$

where Q is the hard scale and μ is a renormalization scale. Here, and throughout this paper, m will represent a generic mass scale on the order of a hadron mass. When different flavors of partons are present, the convolution additionally involves matrix multiplication.

*emoff003@odu.edu
†wmelnitc@jlab.org
‡tedconantrogers@gmail.com
§nsato@jlab.org

(2) Longitudinal momentum. For collinear factorization, the convolution should only be over a longitudinal momentum fraction. The collinear approximations apply to the limit that quantities such as intrinsic transverse momentum or parton virtuality are $O(m)$ and appear only in the power-suppressed error term typically as $O(m^2/Q^2)$.
(3) Universal parton densities. The PDF $f(\xi,\mu)$ has a well-defined operator definition that appears in a diverse class of collinear factorizable processes, and so can be said to be universal. The universality property is especially central to global PDF analyses [2,3].

While the collinear factorization paradigm has been extremely useful in applications at high energies, it is important to examine the extent to which it can be practically utilized at the lower range of energies of interest to studies of hadron structure in QCD, where α_s may be small, but where effects from beyond the usual kinematical collinear approximations become important. Such effects include target mass corrections (TMC), higher twist contributions, or intrinsic k_T and parton virtuality. Strictly speaking, collinear factorization derivations only apply to the limit of small m/Q. Nevertheless, $\alpha_s(Q)/\pi$ remains reasonably small even for values of Q comparable to the nucleon mass. For example, τ-lepton decays with $Q = 1.78$ GeV are used in global extractions of the strong coupling, and find $\alpha_s/\pi \approx 0.1$. [5].

In the case of DIS, processes at scales of a few GeV involve an interesting mixture of perturbative and nonperturbative behavior. For example, some consequences of a small coupling associated with asymptotic freedom, such as approximate Q^2 scaling, persist even at scales low enough for nonperturbative features like resonances to be clearly observable (this is sometimes referred to as "precocious scaling") [6,7]. The observation of scalinglike behavior in certain observables in kinematic regions where hadronic (resonance) degrees of freedom are still prominent is related to the phenomenon of "quark-hadron duality," which characterizes the similarity between low-energy cross sections, averaged over appropriate energy intervals, and those computed from quarks and gluons in perturbative QCD [8–11]. Unraveling the dynamical origin of this behavior remains a challenge for strong interaction physics, and has motivated studies of the nature of the transition from the perturbative to nonperturbative regimes of QCD (for a review, see Ref. [12]). Structure functions in the large-$x_{\rm bj}$ region have also been used to explore the behavior of $\alpha_s(Q)$ in the nonperturbative limit [13].

Many techniques have been put forward for extending the basic collinear factorization framework to accommodate quantitative analyses of data at lower energy or larger $x_{\rm bj}$. Most aim to accommodate small corrections from beyond strict collinearity. One strategy has been to include certain classes of the $O(m/Q)$ corrections in Eq. (1) by arguing that some types of power-suppressed corrections are more important than others. Another has been to perform all-order resummations of terms that involve factors of $\ln(1-x_{\rm bj})$ [14–17]. In some approaches, higher-twist operators in an operator product expansion (OPE) have been able to be kept explicitly [18,19].

Of the various types of $1/Q$ power corrections, TMCs receive particular attention in moderate- to low-Q applications, where M/Q-suppressed effects that are ordinarily neglected in standard collinear factorization become important [20]. The most common approach to quantifying TMCs is based on the pioneering work of Georgi and Politzer [21] and Nachtmann [22]. It re-examines the OPE [23–25] and includes some terms that would usually be marked as power-suppressed, but neglects others such as those associated with quark off-shellness. This framework has been used to evaluate the TMCs for both the spin-averaged [21] and spin-dependent [26] structure functions, at twist-two and twist-three levels [27]. Corrections obtained in this way are often called "kinematical higher twists," to distinguish them from $1/Q$-suppressed "dynamical higher twists" that are associated with multiparton operators in the OPE.

Strictly speaking, it is of course not possible to uniquely decouple all TMCs from dynamical power corrections. This was appreciated already in the early TMC work within the OPE [21,28,29], in the context of the so-called "threshold problem," whereby the target mass corrected structure functions remain nonzero at $x = 1$ [20,30–32]. Later work [18] within a diagrammatic, momentum-space approach extended the collinear factorization framework to lower Q by accounting for multiparton correlations and TMCs up to $O(1/Q^2)$, including the effects of the parton transverse momentum, $k_{\rm T}$. That analysis elucidated the relationship between the parton $k_{\rm T}$ and the parton virtuality, and established a correspondence with the earlier OPE formulation.

Most methods for dealing with target masses are rooted in a fundamentally collinear picture, in that all nonperturbative correlation functions depend only on collinear momentum fractions, with an implicit assumption that corrections to purely collinear kinematics are expressible as a series of powers in m/Q or $\alpha_s(Q)$, or both. For moderately low Q, an alternative possibility is that a hard factor can indeed be identified and expanded in small $\alpha_s(Q)$, but that the associated nonperturbative factors become fundamentally noncollinear. In that case, multiple components of intrinsic nonperturbative parton momentum might need to be included from the outset, not merely in the form of small corrections to collinearity. Parton correlation functions that go beyond the standard inclusive collinear PDFs have a long history, and include objects like transverse momentum dependent (TMD) parton distributions, which include sensitivity to intrinsic transverse components of parton momentum in addition to the usual longitudinal

ones. TMD PDFs are usually used for describing observables, such as in semi-inclusive DIS, that have direct sensitivity to intrinsic parton k_T. However, the particular kinematical scenarios at moderate Q or larger x_{bj} might require similar shifts in the underlying partonic picture, even at the totally inclusive level.

A complication with questions about the limitations of any one approach, or about the advantages of one approach over another, is that it is difficult to precisely estimate the sizes of errors without greater knowledge of nonperturbative QCD than is currently available. Nevertheless, improved methods for estimating the sizes of corrections to factorization theorems are becoming more urgently needed for addressing fundamental theoretical QCD questions in the relatively complicated environment of moderate- to low-Q physics. A hope is that new efforts to understand PDFs from the lattice QCD perspective may help.

The strategy of this paper is based on the observation that most methods for deriving collinear factorization, such as the OPE [23–25], Libby-Sterman style analyses of mass singularities [33], or soft-collinear effective theories [34], apply generally to most simple renormalizable quantum field theories. If a factorization formula is well-behaved in the context of QCD, with all its complications from non-Abelian gauge invariance and confinement, then it should certainly be well-behaved in a much simpler renormalizable field theory without gauge degrees of freedom. We will exploit this by exploring the limitations of factorization derivations in a simple field theory of a quark coupling to a scalar "diquark" to form a "nucleon." We will use this to stress test the standard collinear parton model kinematical approximations.

We will argue, on the basis of the scalar diquark theory, that target masses, quark masses, quark transverse momentum, and quark virtuality are all likely to have similar quantitative importance at momentum scales of order a few GeV. Moreover, the analysis will allow us to propose a factorization-based notion of purely kinematical TMCs. For the lowest Q and largest x_{bj} that typically define the boundary of the DIS region, we find that corrections to a collinear picture are not negligible, and new factorization theorems, with correlation functions that depend on multiple components of parton momentum, may be necessary. Finally, we will illustrate the general usefulness of the scalar diquark theory (or similar models) as a testing ground for the approximations in a factorization derivation. A factorization derivation deals, in essence, directly with a power series expansion of the cross section in m/Q; a factorization theorem is a characterization of the leading power. Factorization is therefore the appropriate context for characterizing the size and general behavior of power corrections.

This paper is organized as follows. In Sec. II we define the scalar diquark theory and discuss its analogy with the pertinent features of QCD. After providing the standard definition of inclusive DIS, the full calculation with exact kinematics is presented in Sec. III. The computation includes all diagrams, to lowest order in the coupling, that are necessary to maintain electromagnetic gauge invariance. We derive nonfactorized expressions for the contributions to the F_1 and F_2 structure functions from the "handbag" topology and $1/Q$-suppressed "cat's ears" diagrams. The standard collinear factorization algorithm is presented in Sec. IV, and the basic steps in the derivation of the collinear PDF are outlined. The results are found to be identical to those of the exact calculation in the $m/Q \to \infty$ limit, but as Q is lowered one is able to study effects from nonvanishing m/Q directly. In Sec. V we study these differences numerically, with the goal of analyzing the relative importance of different types of power corrections at moderate Q, and identifying the regions of kinematics where the collinearly factorized results may provide good approximations to the exact structure functions. Finally, in Sec. VI we summarize our findings and discuss their implications for future analyses.

II. DIS IN A SIMPLE MODEL

A. Definition

We begin by describing the field theory we will use as a proxy for QCD to highlight the salient aspects of factorization approximations at moderate values of Q. Our results mainly concern the kinematics of the process, and complications from the non-Abelian nature of the full QCD theory do not directly affect the general conclusions. The simplified theory is still sufficiently nontrivial that the usual hurdles to deriving factorization in a renormalizable quantum field theory are present.

The theory describes the interaction between a spin-$1/2$ "nucleon" with mass M represented by the field Ψ_N, a spin-$1/2$ "quark" field ψ_q with mass m_q, and a scalar "diquark" state ϕ with mass m_s that does not couple to the photon but remains a spectator to the hard scattering from the quark. The interaction Lagrangian density for this theory is given by a Yukawa-like interaction,

$$\mathcal{L}_{\text{int}} = -\lambda \overline{\Psi}_N \psi_q \phi + \text{H.c.}, \tag{2}$$

where the coupling λ gives the strength of the nucleon-quark-diquark interaction. In this theory, the electron couples to quarks via electroweak gauge bosons as in the standard model. Furthermore, the theory is renormalizable, and the basic derivation of factorization theorems apply equally well to scattering processes here as to processes in QCD, where non-Abelian gauge invariance leads to complications that make factorization derivations more involved. In practice, factorization means that $O(Q)$ physics factorizes from effects sensitive to intrinsic mass scales. The simplified theory is ideal for stress-testing factorization techniques generally before applying them to

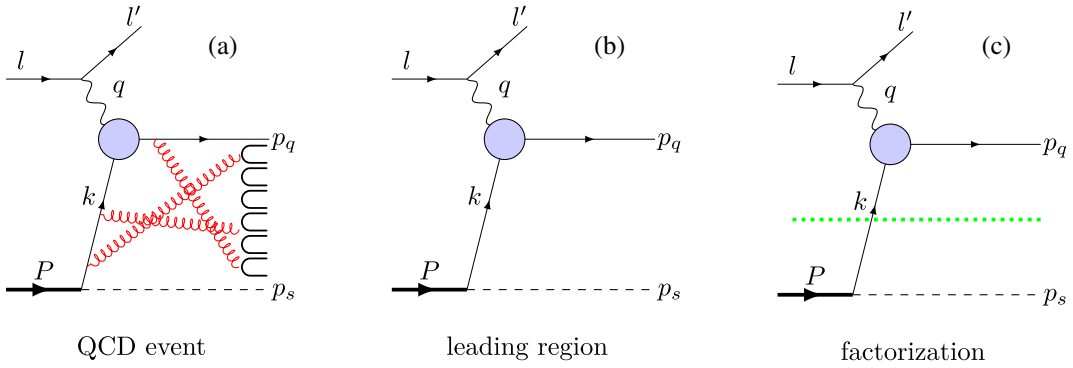

FIG. 1. The sequence of approximations leading to the canonical parton model picture: (a) A physical picture of the complete QCD event. The symbols $\subset$ represent the final state hadronization process. (b) The leading-power topological region contributing to the inclusive cross section. (c) The kinematical approximation (represented by the green dotted horizontal line) that produces the parton model cross section. The line is an instruction to replace the parton momentum by its approximated values (see Sec. IV). The momentum labels are discussed in the text.

the more challenging environment of a non-Abelian gauge theory such as QCD.

B. Analogy with QCD

The model described above is useful only to the extent that it highlights important aspects of actual QCD interactions. This is not a trivial point, since the handbag topology, while a useful starting point, does not strictly capture the true nature of QCD in DIS; a more accurate picture is probably closer to Monte Carlo event generators. Namely, partons generate showers of radiation both before and after the collision, and an arrangement of final state partons undergoes nonperturbative interactions to form a complex array of observable hadrons. This is illustrated in Fig. 1(a). This diagram emphasizes the physical picture of DIS: a sea of parton fluctuations involving quarks, antiquarks, and gluons populates the rapidity interval between the incoming hadron and struck quark rapidities, with the partons interacting nonperturbatively to produce the final state hadrons. [Final state gluons are not shown explicitly in Fig. 1(a).]

The factorization theorem for inclusive scattering states, in part, that the sum of such diagrams may be approximated by the handbag topology of Fig. 1(b) in the limit of large Q. The diagram in Fig. 1(b) belongs to the leading region for inclusive DIS. Finally, a factorization formula emerges once approximations are applied to the active parton momentum, above and below the horizontal line in Fig. 1(c) separating the hard and soft parts of the diagram (see Ref. [35] for more details).

The replacements in Fig. 1, from (a) to (b) and then (b) to (c), are only valid after integration over final states that results in a cascade of cancellations of nonfactorizing effects. The approximations therefore rely on the cross section being fully inclusive. Any map from exact underlying quark and gluon degrees of freedom to the handbag picture is unavoidably indirect. Nevertheless, for the factorization theorem to hold, it is a *necessary* condition that the approximations on parton momentum represented by the horizontal line in Fig. 1(c) be at least roughly accurate. Thus, the transition from (b) to (c) will be the focus of this paper. The main effect of that approximation is simply to alter the kinematics of the handbag diagram. We stress that such approximations are at the core of QCD factorization theorems which can also be studied in the context of the quark-diquark field theory. We will review those approximations in Sec. IV.

In our simple toy field theory, the magnitude of the factorization error is fixed by the sizes of m_q and m_s relative to Q. The same will be true in QCD for the analogous quantities. These parameters determine the size of the small components of parton four-momentum related to k^2 and k_{T}. Other aspects of the quark-diquark theory, such as the dominant k_{T} power law of correlation functions at large k_{T}, are also the same in QCD. The main difference between QCD and the toy theory is that, while the values of m_q and m_s are exactly fixed by the Lagrangian (and by our restriction to the lowest-order graph) in the diquark theory, in QCD the effective parton and spectator masses generally have a spectrum of values that depend on x_{bj}, k_{T}, and Q and intrinsic properties of the nucleon wave function. The kinematically allowed phase space grows with decreasing x_{bj} and increasing Q, accommodating more of the soft radiation sketched in Fig. 1(a). Thus, the scales analogous to m_q and m_s will generally acquire nontrivial x_{bj} and Q dependence in QCD.

In both theories, however, $|k^2|$ and k_{T}^2 need to be small relative to Q^2 to give the m/Q suppression of neglected terms that is necessary for the factorization theorem in Eq. (1) to hold. If m_q and m_s are fixed to reasonable values for a given range of kinematics, and if the integration over k_{T} is dominated by $k_{\mathrm{T}} \ll Q$, then we may verify directly that the parton model approximations are good for the quark-diquark theory. Showing this directly lends some

support to the same approximations in QCD. Conversely, if the approximations fail dramatically in the toy theory, then it is unlikely that they are safe in QCD for the same kinematical region, particularly given the additional complications with non-Abelian gauge invariance, strong coupling, and nonperturbative hadronization.

Carrying this out requires a reasonable set of estimates for m_s and m_q for a specified ranges of kinematics. For $Q\sim$ several GeV, the requirement that m/Q is small implies that m_q should be no larger than several hundred MeV and m_s should be such that $|k^2|$ is also no larger than several hundred MeV for small k_{T}. Unfortunately, there are, to our knowledge, no systematic methods for precisely estimating values for the small components of parton momentum like m_q and $|k^2|$. On the other hand, phenomenological studies of transverse momentum dependence in semi-inclusive DIS suggest typical ranges for these parameters. Extractions of TMD functions find typical magnitudes for the intrinsic transverse momentum width between ≈500 MeV and 800 MeV [36–38]. Since m_q and m_s determine the widths and shapes of the k_{T} distribution, these estimates provide reasonable lower bounds on m_q and m_s. Earlier estimates gave smaller values. For example, a value of $\langle k_{\mathrm{T}}\rangle \sim$ 300 MeV is roughly consistent with both the zero-point energy of bag models as well as nonrelativistic constituent quark models [39], and this is the value quoted in Ref. [21]. It is interesting to ask why phenomenological extractions tend to produce broader nonperturbative distributions than these expectations. (See also the discussion in Ref. [36].) For now we leave this to be addressed in future work.

In this analysis we will use a range of values for m_q and m_s motivated by the above estimates, and examine the sensitivity to their variation for $Q \sim$ 1–2 GeV and moderate x_{bj}. Sensitivity to the exact values of these parameters will be interpreted as a sign that extra care may be needed when estimating their effects on power corrections. We will return to the question of exact values for m_q and m_s in Sec. V A, after examining DIS kinematics in more detail.

C. Structure tensors

Let us review the standard notation of the inclusive DIS process $e(\ell) + N(P) \to e(\ell') + X(p_X)$ in Fig. 1, where ℓ and ℓ' are the initial and final lepton four-momenta, P is the four-momentum of the nucleon, and $p_X = p_q + p_s$ is the four-momentum of the inclusive hadronic state X. It will be convenient for our analysis to work in the Breit frame, where the nucleon moves along the $+z$ direction and the virtual photon moves along the $-z$ axis with zero energy. We will use light-front coordinates, in which a four-vector $v^\mu = (v^+, v^-, \boldsymbol{v}_{\mathrm{T}})$ has "±" components $v^\pm = (v^0 \pm v^z)/\sqrt{2}$ and transverse component $\boldsymbol{v}_{\mathrm{T}}$. The four-momenta of the nucleon and the exchanged photon ($q = \ell - \ell'$) can then be written as

$$P^\mu = \left(\frac{Q}{x_{\mathrm{n}}\sqrt{2}}, \frac{x_{\mathrm{n}} M^2}{Q\sqrt{2}}, \mathbf{0}_{\mathrm{T}}\right), \tag{3}$$

$$q^\mu = \left(-\frac{Q}{\sqrt{2}}, \frac{Q}{\sqrt{2}}, \mathbf{0}_{\mathrm{T}}\right), \tag{4}$$

where $Q \equiv \sqrt{-q^2}$ is the magnitude of the four-momentum transfer, and

$$x_{\mathrm{bj}} \equiv \frac{Q^2}{2P\cdot q}, \tag{5}$$

$$x_{\mathrm{n}} \equiv -\frac{q^+}{P^+} = \frac{2x_{\mathrm{bj}}}{1+\sqrt{1+4x_{\mathrm{bj}}^2 M^2/Q^2}} \tag{6}$$

are the Bjorken and Nachtmann scaling variables, respectively. The Bjorken variable x_{bj} can also be written in terms of the Nachtmann variable,

$$x_{\mathrm{bj}} = \frac{x_{\mathrm{n}}}{(1 - x_{\mathrm{n}}^2 M^2/Q^2)}. \tag{7}$$

Considering the leading region, Fig. 1(b), the final state quark (or "jet") momentum is p_q, and the momentum of the spectator system is p_s, with

$$p_q^2 = m_q^2, \qquad p_s^2 = m_s^2. \tag{8}$$

We also define a momentum transfer variable,

$$k \equiv p_q - q = P - p_s. \tag{9}$$

In a handbag diagram [see Fig. 2(a) below], k would be the momentum of the incoming struck quark. The invariant mass squared of the photon-nucleon system is

$$W^2 = (P+q)^2 = (p_q + p_s)^2 = M^2 + \frac{Q^2(1-x_{\mathrm{bj}})}{x_{\mathrm{bj}}}. \tag{10}$$

The boost-invariant cross section for the inclusive DIS process is

$$E'\frac{\mathrm{d}\sigma}{\mathrm{d}^3\ell'} = \frac{\alpha^2}{2\pi(s-M^2)Q^4} L_{\mu\nu} W^{\mu\nu}, \tag{11}$$

where α is the electromagnetic fine structure constant, E' is the final lepton energy, and s is the usual Mandelstam variable. The only approximation is to neglect the lepton mass in the flux factor. The leptonic tensor is $L_{\mu\nu} = 2(\ell_\mu \ell'_\nu + \ell'_\mu \ell_\nu - g_{\mu\nu}\ell\cdot\ell')$ is the leptonic tensor. We are most interested in the hadronic tensor,

$$W^{\mu\nu}(P,q) = \sum_X \langle P,S|j^\mu(0)|X\rangle\langle X|j^\nu(0)|P,S\rangle \times (2\pi)^4\delta^{(4)}(P+q-p_X), \tag{12}$$

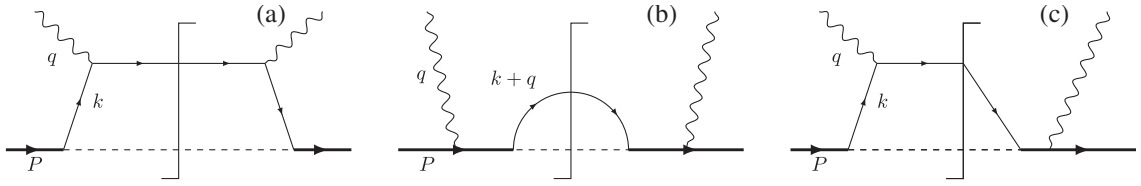

FIG. 2. Contributions to the hadronic tensor from diagrams allowed by the interaction Lagrangian (2) to $O(\alpha\lambda^2)$ in the couplings. Graph (a) is a manifestation of the familiar handbag diagram and represents the topology of the leading region. Graphs (b) and (c) are suppressed by powers of $1/Q$ when $k_{\rm T}$ is small, but are needed for gauge invariance. The Hermitian conjugate for (c) is not shown. The momenta on the various legs are as indicated.

where Σ_X represents the inclusive integration over all hadronic final states with overall four-momentum p_X. Note that all factors of α appear in the prefactor in Eq. (11). Also, we have moved a conventional $1/(4\pi)$ factor from the definition of the hadronic tensor into the overall factor in Eq. (11) to minimize the number of factors of π that need to be accounted for in intermediate steps. For the scattering of an unpolarized lepton from an unpolarized nucleon, the hadronic tensor $W^{\mu\nu}$ is usually expressed in terms of the spin-averaged structure functions F_1 and F_2,

$$W^{\mu\nu}(P,q) = \left(-g^{\mu\nu} + \frac{q^\mu q^\nu}{q^2}\right) F_1(x_{\rm n}, Q^2) + \left(P^\mu - \frac{P\cdot q}{q^2} q^\mu\right)\left(P^\nu - \frac{P\cdot q}{q^2} q^\nu\right)\frac{F_2(x_{\rm n}, Q^2)}{P\cdot q}. \tag{13}$$

The structure functions are obtained from the hadronic tensor by applying projection operators,

$$F_i(x_{\rm n}, Q^2) = \mathrm{P}_i^{\mu\nu} W_{\mu\nu}(P,q), \qquad i = 1,2, \tag{14}$$

where

$$\mathrm{P}_1^{\mu\nu} = -\frac{1}{2}\mathrm{P}_g^{\mu\nu} + \frac{2Q^2 x_{\rm n}^2}{(M^2 x_{\rm n}^2 + Q^2)^2}\mathrm{P}_{PP}^{\mu\nu}, \tag{15a}$$

$$\mathrm{P}_2^{\mu\nu} = \frac{12Q^4 x_{\rm n}^3 (Q^2 - M^2 x_{\rm n}^2)}{(Q^2 + M^2 x_{\rm n}^2)^4}\left(\mathrm{P}_{PP}^{\mu\nu} - \frac{(M^2 x_{\rm n}^2 + Q^2)^2}{12Q^2 x_{\rm n}^2}\mathrm{P}_g^{\mu\nu}\right), \tag{15b}$$

with the components

$$\mathrm{P}_g^{\mu\nu} = g^{\mu\nu}, \qquad \mathrm{P}_{PP}^{\mu\nu} = P^\mu P^\nu. \tag{16}$$

See Ref. [40] for a full structure decomposition of SIDIS with spin and azimuthal dependence and exact kinematics.

In Eq. (13) we have written the structure functions in terms of the Nachtmann $x_{\rm n}$ variable instead of Bjorken $x_{\rm bj}$, as is more commonly presented in the literature. The reason is that $x_{\rm n}$ is the natural scaling variable in the parton model approximation $k^+ \approx -q^+$ when M is not set to zero. In the limit that power-suppressed terms can be dropped, the two scaling variables are equal,

$$x_{\rm n} = x_{\rm bj} + O\left(\frac{x_{\rm bj}^2 M^2}{Q^2}\right), \tag{17}$$

although we stress that the $x_{\rm n} \approx x_{\rm bj}$ approximation is not generally necessary and is separate from the approximations needed to factorize short- and long-distance physics in a theory with interactions. Both $\{x_{\rm n}, Q\}$ and $\{x_{\rm bj}, Q\}$ are equally valid as independent kinematic variables; since $x_{\rm n}$ is the natural variable when hadron masses are not neglected, we will use it everywhere unless specified otherwise.

III. EXACT KINEMATICS

Having defined the model and the quantities of interest, in this section we calculate the DIS structure functions from the Lagrangian $\mathcal{L}_{\rm int}$ in Eq. (2) at the lowest nontrivial order, $O(\alpha\lambda^2)$. The corresponding graphs derived from $\mathcal{L}_{\rm int}$ are shown in Fig. 2. Graph (a) has the familiar handbag diagram topology, while graphs (b) and (c) are power-suppressed at large Q but are needed for exact electromagnetic gauge invariance—see Appendix A. We exclude the elastic limit of $x_{\rm bj} = 1$ and require strictly $W > M$, so that diagrams with an on-shell nucleon in the final state are forbidden.

Graphs (b) and (c) represent the direct coupling of the photon to the nucleon, with production of a far off-shell nucleon in the intermediate state. In the quark-diquark field theory the coupling is pointlike, while in QCD it corresponds to a higher-twist interaction internal to the nucleon wave function, with the final state quark interacting with the nucleon remnant to form a highly virtual intermediate state.

We begin by presenting the organization of the calculation of the graphs in Fig. 2, with no approximations whatsoever on kinematics. Of course, the result will not be factorized. Later, we will compare with the canonical parton model approximations that factorize the graphs into a hard collision and a PDF contribution.

The exact calculation is organized by separating the integrand of the hadronic tensor into factors representing different parts of the squared amplitude,

$$W^{\mu\nu}(P,q) = \sum_{j\in\text{graphs}} \frac{1}{2}\int \frac{\mathrm{d}k^+ \mathrm{d}k^- \mathrm{d}^2\boldsymbol{k}_{\rm T}}{(2\pi)^2}\,[\mathrm{Jac}]\,\mathrm{T}_j^{\mu\nu}\,[\mathrm{Prop}]_j \times \delta(k^- - k^-_{\rm sol})\,\delta(k^+ - k^+_{\rm sol}), \tag{18}$$

where k is the four-momentum of the interacting parton, and the sum over j runs over the graphs labeled by $j \in \{a, b, c\}$. The propagator denominators in Eq. (18) have been gathered into the factor $[\mathrm{Prop}]_j$, and the traces over the γ matrices are denoted by $\mathrm{T}_j^{\mu\nu}$. The resulting Jacobian factor associated with the integration over $k^\pm$ is denoted as [Jac]. To simplify notation, we will fix $\lambda = \sqrt{2}$ and drop all explicit factors of λ^2 throughout the rest of this article. The δ functions stem from the on-shell conditions for the final state quark and scalar diquark,

$$(q+k)^2 - m_q^2 = 0, \tag{19a}$$

$$(P-k)^2 - m_s^2 = 0. \tag{19b}$$

Solving this system of equations for $k^+ \equiv \xi P^+$ and k^- gives two solutions for k^-. In the limit of $Q \to \infty$ with x_n and k_T fixed, the two solutions behave as $k^- \sim \infty$ and $k^- \sim 0$, respectively. Selecting the latter as the physically relevant solution for DIS, we obtain the values of the light-cone parton momenta $k^\pm_\mathrm{sol}$ with on-shell final state quark and diquark,

$$k^- = k^-_\mathrm{sol} \equiv \frac{\sqrt{\Delta} - Q^2(1-x_\mathrm{n}) - x_\mathrm{n}(m_s^2 - m_q^2 - M^2(1-x_\mathrm{n}))}{2\sqrt{2}Q(1-x_\mathrm{n})}, \tag{20a}$$

$$k^+ = k^+_\mathrm{sol} \equiv \frac{k_\mathrm{T}^2 + m_q^2 + Q(Q+\sqrt{2}k^-)}{\sqrt{2}(Q+\sqrt{2}k^-)}, \tag{20b}$$

where $k_\mathrm{T}^2 = \boldsymbol{k}_\mathrm{T}^2$, and the discriminant Δ is

$$\begin{aligned}\Delta = {} & [Q^2(1-x_\mathrm{n}) - x_\mathrm{n}(M^2(1-x_\mathrm{n}) + m_q^2 - m_s^2)]^2 \\ & - 4x_\mathrm{n}(1-x_\mathrm{n})[k_\mathrm{T}^2(Q^2 + x_\mathrm{n}M^2) - Q^2M^2(1-x_\mathrm{n}) \\ & + Q^2 m_s^2 + x_\mathrm{n}M^2 m_q^2].\end{aligned} \tag{21}$$

The parton virtuality is obtained by substituting Eqs. (20a)–(20b) into

$$k^2 = 2k^+k^- - k_\mathrm{T}^2. \tag{22}$$

The Jacobian factor in Eq. (18) is

$$[\mathrm{Jac}] = \frac{x_\mathrm{n}Q(2k^- + \sqrt{2}Q)}{4(1-x_\mathrm{n})k^-Q^2(\sqrt{2}k^- + 2Q) + 2\sqrt{2}[Q^4(1-x_\mathrm{n}) - (k_\mathrm{T}^2 + m_q^2)x_\mathrm{n}(Q^2 + x_\mathrm{n}M^2)]}. \tag{23}$$

For this article, we are interested in the small-$|k^2|$ region where a parton model approximation might be reasonable. The k^- solution corresponding to large $|k^2|$ is dealt with in an $O(\lambda^2)$ treatment of the hard part. The exact propagator factors for each of the contributions in Fig. 2 are

$$[\mathrm{Prop}]_a = \frac{1}{(k^2 - m_q^2)^2}, \tag{24a}$$

$$[\mathrm{Prop}]_b = \frac{1}{((P+q)^2 - M^2)^2} = \frac{x_\mathrm{n}^2}{(Q^2(1-x_\mathrm{n}) - M^2x_\mathrm{n}^2)^2}, \tag{24b}$$

$$[\mathrm{Prop}]_c = \frac{1}{(k^2 - m_q^2)} \frac{x_\mathrm{n}}{(Q^2(1-x_\mathrm{n}) - M^2x_\mathrm{n}^2)}. \tag{24c}$$

The numerator factors $\mathrm{T}_j^{\mu\nu} = \mathrm{T}_j^{\mu\nu}(P, k, m_q, m_s)$ are obtained from the Dirac traces in each graph in Fig. 2,

$$\mathrm{T}_a^{\mu\nu} = \mathrm{Tr}[(\not{P} + M)(\not{k} + m_q)\gamma^\mu(\not{k} + \not{q} + m_q)\gamma^\nu(\not{k} + m_q)], \tag{25a}$$

$$\mathrm{T}_b^{\mu\nu} = \mathrm{Tr}[(\not{P} + M)\gamma^\mu(\not{P} + \not{q} + M)(\not{k} + \not{q} + m_q)(\not{P} + \not{q} + M)\gamma^\nu], \tag{25b}$$

$$\mathrm{T}_c^{\mu\nu} = 2\mathrm{Tr}[(\not{P} + M)(\not{k} + m_q)\gamma^\mu(\not{k} + \not{q} + m_q)(\not{P} + \not{q} + M)\gamma^\nu], \tag{25c}$$

where the factor of 2 in $\mathrm{T}_c^{\mu\nu}$ accounts for the Hermitian conjugate of Fig. 2(c). In evaluating the traces Eq. (23), it will be convenient to define the projected quantities

$$\mathrm{T}_j^g = \mathrm{P}_g^{\mu\nu}\mathrm{T}_{j\mu\nu}, \qquad \mathrm{T}_j^{PP} = \mathrm{P}_{PP}^{\mu\nu}\mathrm{T}_{j\mu\nu}. \tag{26}$$

Evaluating the projections explicitly,

$$\mathrm{T}_a^g = -8[2(P\cdot k + m_q M)k\cdot q + (k^2 - 3m_q^2)P\cdot k - 2Mm_q^3 + (m_q^2 - k^2)P\cdot q], \tag{27a}$$

$$\begin{aligned}\mathrm{T}_b^g = 8[&2M^3 m_q + P\cdot k(2M^2 - Q^2) - 2(M^2 + Mm_q)Q^2 \\ &+ 2k\cdot q(M^2 - P\cdot q) + [2(M^2 + Mm_q) + Q^2]P\cdot q],\end{aligned} \tag{27b}$$

$$\begin{aligned}\mathrm{T}_c^g = -16[&-2(P\cdot k)^2 + k^2M^2 + (M^2 - m_q M)k\cdot q - M^2 m_q^2 + 2Mm_q Q^2 \\ &+ (m_q^2 - Mm_q)P\cdot q - 2P\cdot k(k\cdot q + Mm_q - Q^2 + P\cdot q)],\end{aligned} \tag{27c}$$

$$\begin{aligned}\mathrm{T}_a^{PP} = 4[&4(P\cdot k)^3 + 4(P\cdot k)^2(Mm_q + P\cdot q) \\ &- MP\cdot k(3k^2M + 2Mk\cdot q - 3Mm_q^2 - 4m_q P\cdot q) \\ &- M^3 m_q(k^2 + 2k\cdot q - m_q^2) - M^2(k^2 - m_q^2)P\cdot q],\end{aligned} \tag{27d}$$

$$\begin{aligned}\mathrm{T}_b^{PP} = 4M^2[&P\cdot k(4M^2 + Q^2) + 4M^2(k\cdot q + Mm_q) - Q^2(4M^2 + Mm_q) \\ &+ [2k\cdot q + 4(M^2 + Mm_q) - Q^2]P\cdot q],\end{aligned} \tag{27e}$$

$$\begin{aligned}\mathrm{T}_c^{PP} = 8M[&4M(P\cdot k)^2 + MP\cdot k(2k\cdot q + 4Mm_q - Q^2) \\ &- M^2[2M(k^2 + k\cdot q - m_q^2) + m_q Q^2] \\ &- [k^2M - (2M + m_q)(2P\cdot k + Mm_q)]P\cdot q].\end{aligned} \tag{27f}$$

Putting all the components together, the exact nucleon structure functions $F_{1,2}$ can be written in terms of the k_T-unintegrated distributions,[1]

$$F_1(x_\mathrm{n}, Q^2) = \int \frac{\mathrm{d}^2\boldsymbol{k}_\mathrm{T}}{(2\pi)^2}\mathcal{F}_1(x_\mathrm{n}, Q^2, k_\mathrm{T}^2), \tag{28a}$$

$$F_2(x_\mathrm{n}, Q^2) = \int \frac{\mathrm{d}^2\boldsymbol{k}_\mathrm{T}}{(2\pi)^2}2x_\mathrm{n}\mathcal{F}_2(x_\mathrm{n}, Q^2, k_\mathrm{T}^2), \tag{28b}$$

where

$$\mathcal{F}_1(x_\mathrm{n}, Q^2, k_\mathrm{T}^2) = [\mathrm{Jac}]\sum_j\left(-\frac{1}{2}\mathrm{T}_j^g + \frac{2Q^2x_\mathrm{n}^2}{(M^2x_\mathrm{n}^2 + Q^2)^2}\mathrm{T}_j^{PP}\right)[\mathrm{Prop}]_j, \tag{29a}$$

$$\begin{aligned}2x_\mathrm{n}\mathcal{F}_2(x_\mathrm{n}, Q^2, k_\mathrm{T}^2) = &\frac{12Q^4x_\mathrm{n}^3(Q^2 - M^2x_\mathrm{n}^2)}{(Q^2 + M^2x_\mathrm{n}^2)^4} \\ &\times [\mathrm{Jac}]\sum_j\left(\mathrm{T}_j^{PP} - \frac{(M^2x_\mathrm{n}^2 + Q^2)^2}{12Q^2x_\mathrm{n}^2}\mathrm{T}_j^g\right)[\mathrm{Prop}]_j.\end{aligned} \tag{29b}$$

For later convenience, the function $\mathcal{F}_2$ in Eqs. (28b) and (29b) has been defined with a factor $2x_\mathrm{n}$ pulled out in order to more directly compare the behavior of the k_T dependence of the k_T-unintegrated functions (see Sec. V below).

Note that exact kinematics impose a specific upper bound on k_T. To determine its value, write W in the center-of-mass (c.m.) system,

$$W = p_q^0 + p_s^0\Big|_{\mathrm{c.m.}} = \sqrt{m_q^2 + k_\mathrm{T}^2 + k_z^2} + \sqrt{m_s^2 + k_\mathrm{T}^2 + k_z^2}\Big|_{\mathrm{c.m.}}. \tag{30}$$

For fixed external kinematics, the maximum k_T occurs when $k_z = 0$. Setting

$$\sqrt{m_q^2 + k_{\mathrm{T}\,\mathrm{max}}^2} + \sqrt{m_s^2 + k_{\mathrm{T}\,\mathrm{max}}^2} = W \tag{31}$$

[1]Note that these are not PDFs, which are only defined after factorizing approximations are applied.

and solving for $k_{\mathrm{T\,max}}$ gives

$$k_{\mathrm{T\,max}} = \sqrt{\frac{[x_{\mathrm{bj}}(M^2-(m_q+m_s)^2)+Q^2(1-x_{\mathrm{bj}})][x_{\mathrm{bj}}(M^2-(m_q-m_s)^2)+Q^2(1-x_{\mathrm{bj}})]}{4x_{\mathrm{bj}}[Q^2(1-x_{\mathrm{bj}})+M^2x_{\mathrm{bj}}]}}, \tag{32}$$

where Eq. (10) has been used for W. Results for the exact structure functions will be shown in Sec. V.

IV. FACTORIZATION

In this section, we review the minimal kinematic approximations needed for standard factorization with low-order handbag graphs such as in Fig. 3. More details with extensive discussion of the justification for the applicability of factorization may be found, for example, in Sec. 6.1.1 of Ref. [35].

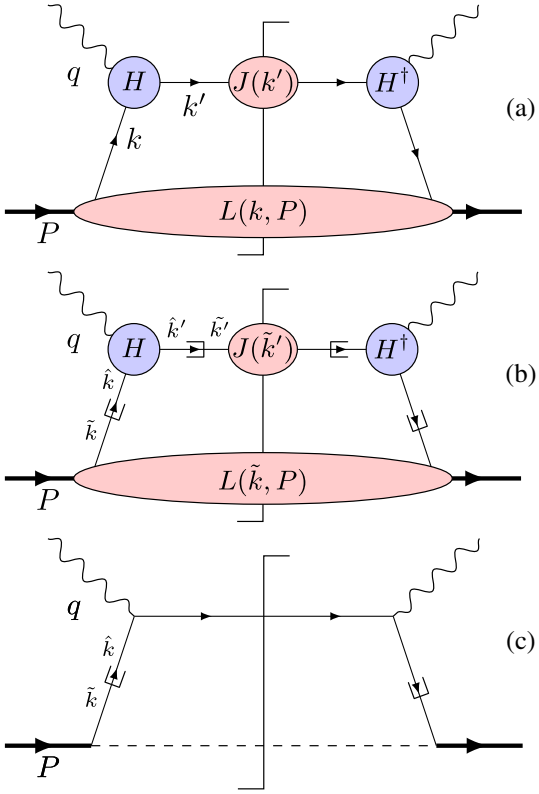

FIG. 3. The steps in the usual factorization approximation applied to a handbag topology. (a) Unapproximated handbag topology, with H denoting the hard scattering of a virtual photon from a quark with momentum k to one with momentum $k' = k + q$, $J(k')$ is the jet function, and $L(k, P)$ is the soft target amplitude. (b) Handbag diagram with standard factorization, with the parton momentum approximated by $\hat{k}$ in the hard function H, and by $\tilde{k}$ in the jet and soft functions. The hooks represent the point of application of kinematic approximations on parton momentum. (c) Application of the $O(\lambda^2)$ contribution in the theory from Sec. II.

The first step in a collinear factorization derivation in DIS is to identify and restrict attention to leading (in m/Q) region graphical topologies. One such configuration, and the only one contributing at zeroth order coupling in the hard part, is the handbag topology of Fig. 3(a), with two final state jets: one with momentum $k' = k + q$, and the other with momentum $P - k$. The "cat's ears" graph topologies, corresponding to Figs. 2(b) and 2(c), are suppressed by powers of $1/Q^2$ and so do not contribute in the leading power approximation.

The contribution to the hadronic tensor from the amplitude in Fig. 3(a) has the general form

$$W^{\mu\nu}(P,q) = \int \frac{\mathrm{d}^4k}{(2\pi)^4}\mathrm{Tr}[H^{\mu}(k,k')J(k')H^{\nu\dagger}(k,k')L(k,P)]. \tag{33}$$

Here $H^{\mu}(k,k')$ and $H^{\nu\dagger}(k,k')$ represent the hard scattering blobs in Fig. 3(a), where all internal lines off-shell by at least $O(Q^2)$. The target, $L(k,P)$, and jet, $J(k')$, blobs have internal lines off-shell by $O(m^2)$, where the generic hadronic mass scale $m \in \{m_q, m_s, M\}$. The parton lines that connect the various blobs have small off-shellness, with k^2 and $k'^2 \sim O(m^2)$. In the Breit frame $k^+ \sim O(Q)$. The low transverse momentum region is where $k_{\mathrm{T}} \sim O(\boldsymbol{m}_{\mathrm{T}})$, where $\boldsymbol{m}_{\mathrm{T}}$ denotes the transverse momentum components of the parton momentum, each of which is of $O(m)$. The power counting for the struck parton momentum is therefore

$$k \sim \left(O(Q), O\left(\frac{m^2}{Q}\right), O(\boldsymbol{m}_{\mathrm{T}})\right). \tag{34}$$

We remind the reader that m symbolizes any typical hadronic mass scale. To factorize the cross section, one exploits Eq. (34) to justify a standard set of kinematic approximations that we now review.

In the hard subgraphs, terms proportional to k^2 or k'^2 are small relative to the $O(Q^2)$ off-shellness of the propagators. Since $k \cdot q = k^+q^- + O(m^2)$, the replacement of $k \cdot q \to k^+q^-$ in the hard blobs therefore introduces only $O(m^2/Q^2)$ suppressed errors at small k_{T}. Thus, the momenta in the hard parts are replaced by partonic "hatted" variables $\hat{k}$ and $\hat{k}'$,

$$k \to \hat{k} \equiv (\hat{k}^+, 0, \mathbf{0}_\mathrm{T}); \qquad M^2/Q^2 \to 0, \tag{35a}$$

$$k' \to \hat{k}' = \hat{k} + q, \tag{35b}$$

with

$$\hat{k}^2 = \hat{k}'^2 = 0. \tag{35c}$$

These equations give

$$\hat{k}^+ = x_\mathrm{n} P^+ \overset{x_\mathrm{n} \to x_\mathrm{bj}}{=} x_\mathrm{bj} P^+, \tag{36a}$$

$$\hat{k}' = (0, q^-, \mathbf{0}_\mathrm{T}). \tag{36b}$$

The replacement $H^\mu(k,k') \to H^\mu(\hat{k},\hat{k}')$ is therefore a good approximation up to $O(m^2/Q^2)$ corrections. (The replacement of x_n by x_bj is not necessary to obtain factorization, but it is conventional to use x_bj.)

Internal lines in the lower blob $L(k,P)$ are off-shell by $O(m^2)$. With the replacement of $k^+ \to x_\mathrm{bj}P^+ + O(m^2/Q)$,

$$k^2 = 2k^+k^- - k_\mathrm{T}^2 = \underbrace{2(x_\mathrm{bj}P^+)k^- - k_\mathrm{T}^2}_{O(m^2)} + O(m^4/Q^2), \tag{37}$$

$$\begin{aligned}(P+k)^2 &= M^2 + 2P^+k^- + 2P^-k^+ + 2k^+k^- - k_\mathrm{T}^2 \\ &= \underbrace{M^2 + 2P^+k^- + 2P^-(x_\mathrm{bj}P^+) + 2(x_\mathrm{bj}P^+)k^- - k_\mathrm{T}^2}_{O(m^2)} \\ &\quad + O(m^4/Q^2),\end{aligned} \tag{38}$$

where the underbraces collect terms that are $O(m^2)$, and the errors induced by approximating k^+ are $O(m^4/Q^2)$. Therefore, the small components k^- and k_T must be kept exact to avoid introducing unsuppressed errors. Implementing this approximation requires another momentum four-vector $\tilde{k}^\mu$, defined in the Breit frame as

$$\tilde{k} \equiv (x_\mathrm{bj}P^+, k^-, \boldsymbol{k}_\mathrm{T}), \tag{39}$$

so that the replacement $L(k,P) \to L(\tilde{k},P)$ is a good approximation up to terms suppressed by powers of $O(m^2/Q^2)$.

Similarly, the internal lines of $J(k')$ are off-shell by $O(m^2)$, while the power counting for k' is

$$k' \sim (O(Q), O(Q), O(\boldsymbol{m}_\mathrm{T})). \tag{40}$$

To find a suitable approximation, consider a frame labeled by "$*$," where the outgoing transverse momentum vanishes, $k_\mathrm{T}^* = 0$. In terms of the Breit frame variables, one has

$$k'^* = \left(k^+ + q^+ - \frac{k_\mathrm{T}^2}{2(q^- + k^-)}, q^- + k^-, \mathbf{0}_\mathrm{T}\right), \tag{41}$$

so that the outgoing parton's virtuality is

$$\begin{aligned}k'^{*2} &= 2(k^+ + q^+)(k^- + q^-) - k_\mathrm{T}^2 \\ &\sim 2(k^+ + q^+)q^- - k_\mathrm{T}^2 + O\left(\frac{m^3}{Q}\right).\end{aligned} \tag{42}$$

Therefore, the smallest component of k, namely k^-, can be neglected in $J(k')$. To implement this approximation we define the approximate outgoing momentum four-vector

$$k' \to \tilde{k}' \equiv (l^+, q^-, \mathbf{0}_\mathrm{T}), \tag{43}$$

where $l^+ \equiv k^+ - x_\mathrm{bj}P^+ + k_\mathrm{T}^2/(2q^-)$. Changing the integration variables from k^+ to l^+ in Eq. (33) gives

$$W^{\mu\nu}(P,q) = \int \frac{\mathrm{d}l^+ \mathrm{d}k^- \mathrm{d}^2\boldsymbol{k}_\mathrm{T}}{(2\pi)^4} \mathrm{Tr}[H^\mu(Q^2) J(l^+) H^{\dagger\nu}(Q^2) L(\tilde{k},P)] + O\left(\frac{m^2}{Q^2}\right) W^{\mu\nu}. \tag{44}$$

The integrations can now be pushed into separate factors for the target and jet blobs,

$$W^{\mu\nu}(P,q) = \mathrm{Tr}\left[H^\mu(Q^2)\left(\int \frac{\mathrm{d}l^+}{2\pi} J(l^+)\right) H^{\nu\dagger}(Q^2)\left(\int \frac{\mathrm{d}k^- \mathrm{d}^2\boldsymbol{k}_\mathrm{T}}{(2\pi)^3} L(\tilde{k},P)\right)\right] + O\left(\frac{m^2}{Q^2}\right) W^{\mu\nu}. \tag{45}$$

To complete the factorization, the jet and target blobs are decomposed in a basis of Dirac matrices,

$$J(l^+) = \gamma_\mu \Delta^\mu(l^+) + \Delta_S(l^+) + \gamma_5 \Delta_P(l^+) + \gamma_5\gamma_\mu \Delta_A^\mu(l^+) + \sigma_{\mu\nu}\Delta_T^{\mu\nu}(l^+), \tag{46a}$$

$$L(\tilde{k},P) = \gamma_\mu \Phi^\mu(\tilde{k},P) + \Phi_S(\tilde{k},P) + \gamma_5 \Phi_P(\tilde{k},P) + \gamma_5\gamma_\mu \Phi_A^\mu(\tilde{k},P) + \sigma_{\mu\nu}\Phi_T^{\mu\nu}(\tilde{k},P), \tag{46b}$$

in terms of vector, scalar, pseudoscalar, axial vector and tensor functions. If we focus only on spin- and azimuthally independent cross sections, only the first term in Eq. (46a) and the first term in Eq. (46b) need be kept. To leading power,

only the "−" component of Δ^μ and only the "+" component of Φ^μ contribute, so that the jet and target operators can be expanded as

$$J(l^+) = \gamma^+\Delta^-(l^+) + O\left(\frac{m^2}{Q^2}\right)J + (\text{spin dep})$$
$$= \frac{\hat{k}'}{4q^-}\mathrm{Tr}[\gamma^- J(l^+)] + O\left(\frac{m^2}{Q^2}\right)J + (\text{spin dep}), \tag{47a}$$

$$L(\tilde{k}, P) = \gamma^-\Phi^+(\tilde{k}, P) + O\left(\frac{m^2}{Q^2}\right)L + (\text{spin dep})$$
$$= \frac{\hat{k}}{4x_{\mathrm{n}}P^+}\mathrm{Tr}[\gamma^+ L(\tilde{k}, P)] + O\left(\frac{m^2}{Q^2}\right)L + (\text{spin dep}), \tag{47b}$$

where the spin-dependent terms are not written explicitly. Using Eqs. (45), the spin-averaged hadronic tensor is then

$$W^{\mu\nu}(P,q) = \frac{2\pi}{2Q^2}\mathrm{Tr}[H^\mu(Q^2)\hat{k}'H^{\dagger\nu}(Q^2)\hat{k}]\left(\int\frac{\mathrm{d}l^+}{2\pi}\mathrm{Tr}\left[\frac{\gamma^-}{2}J(l^+)\right]\right)$$
$$\times\left(\int\frac{\mathrm{d}k^-\mathrm{d}^2\boldsymbol{k}_{\mathrm{T}}}{(2\pi)^3}\mathrm{Tr}\left[\frac{\gamma^+}{2}L(\tilde{k},P)\right]\right) + O\left(\frac{m^2}{Q^2}\right)W^{\mu\nu}. \tag{48}$$

Finally, the integration contour for l^+ is deformed away from the k' pole until l^+q^- is $O(Q^2)$. To lowest order in λ^2, J can then be replaced by the massless, on-shell cut diagram, so the hadronic tensor in Eq. (48) becomes

$$W^{\mu\nu}(P,q) = \underbrace{\frac{2\pi}{2Q^2}\mathrm{Tr}[H^\mu(Q^2)\hat{k}'H^{\dagger\nu}(Q^2)\hat{k}]}_{\mathcal{H}^{\mu\nu}(Q^2)}\underbrace{\left(\int\frac{\mathrm{d}k^-\mathrm{d}^2\boldsymbol{k}_{\mathrm{T}}}{(2\pi)^4}\mathrm{Tr}\left[\frac{\gamma^+}{2}L(\tilde{k},P)\right]\right)}_{f(x_{\mathrm{bj}})} + O\left(\frac{m^2}{Q^2}\right)W^{\mu\nu}. \tag{49}$$

This is the standard factorized hadronic tensor. The hard scattering factor $\mathcal{H}^{\mu\nu}(Q^2)$ contains the short-distance $[O(Q^2)]$ physics, and the parton distribution $f(x_{\mathrm{bj}})$ contains large-distance $[O(m^2)]$ physics associated with the initial bound state. The transition from Eq. (33) to Eq. (49) is represented graphically in Fig. 3(a)–(c).

From the hadronic tensor, one recovers the structure functions in the collinear (parton model) approximation,

$$F_i(x_{\mathrm{bj}}, Q^2) = \mathcal{H}_i(Q^2)f(x_{\mathrm{bj}}) + O\left(\frac{m^2}{Q^2}\right), \qquad i = 1, 2, \tag{50}$$

where

$$\mathcal{H}_i(Q^2) \equiv \mathrm{P}_i^{\mu\nu}\frac{2\pi}{2Q^2}\mathrm{Tr}[H_\mu(Q^2)\hat{k}'H_\nu^\dagger(Q^2)\hat{k}]. \tag{51}$$

The hard amplitude H^μ is $H^\mu(Q^2) = \gamma^\mu$, so that the projected hard functions in Eq. (51) become

$$\mathcal{H}_1(Q^2) = 2\pi, \tag{52a}$$

$$\mathcal{H}_2(Q^2) = 4\pi\frac{Q^2x_{\mathrm{bj}}(Q^2 - M^2x_{\mathrm{bj}}^2)}{(Q^2 + M^2x_{\mathrm{bj}}^2)^2}$$
$$= 4\pi x_{\mathrm{bj}}\left(1 + O\left(\frac{M^2x_{\mathrm{bj}}^2}{Q^2}\right)\right). \tag{52b}$$

The hadronic tensor in Eq. (12) is often defined with an overall $1/(4\pi)$. Including this in Eq. (50) produces the familiar $F_1 = f(x_{\mathrm{bj}})/2$ and $F_2 = x_{\mathrm{bj}}f(x_{\mathrm{bj}})$ result of the parton model.

In the limit of large Q and at fixed x_{bj}, the graphs in Figs. 2(b) and 2(c) are suppressed by powers of m/Q, and the structure function in the factorized approximation comes entirely from the contribution in Fig. 2(a). The graphical topology is a specific instance of the handbag diagram in Fig. 3(c).

The PDF $f(x_{\mathrm{bj}})$, which describes the lower blob in Fig. 3(a) in the factorized approximation, is

$$f(x_{\rm bj}) = \int \frac{{\rm d}k^- {\rm d}^2\boldsymbol{k}_{\rm T}}{(2\pi)^4} \left(\frac{1}{\tilde{k}^2 - m_q^2}\right)^2 \times {\rm Tr}\left[\frac{\gamma^+}{2}(\tilde{\not{k}} + m_q)(\not{P} + M)(\tilde{\not{k}} + m_q)\right] \times (2\pi)\delta_+((P - \tilde{k})^2 - m_s^2). \quad (53)$$

The on-shell δ function eliminates the integration over k^-, giving

$$k^- = -\frac{x_{\rm bj}[k_{\rm T}^2 + m_s^2 + (x_{\rm bj} - 1)M^2]}{\sqrt{2}Q(1 - x_{\rm bj})}, \quad (54)$$

and the parton virtuality becomes

$$\tilde{k}^2 = -\frac{k_{\rm T}^2 + x_{\rm bj}[m_s^2 + (x_{\rm bj} - 1)M^2]}{1 - x_{\rm bj}}. \quad (55)$$

Finally, the $k_{\rm T}$-unintegrated functions $\mathcal{F}_{1,2}$ defined in Eqs. (26) are given, in the collinear factorization approximation, by

$$\mathcal{F}_1(x_{\rm bj}, Q^2, k_{\rm T}^2) = \mathcal{F}_2(x_{\rm bj}, Q^2, k_{\rm T}^2) = \frac{(1 - x_{\rm bj})[k_{\rm T}^2 + (m_q + x_{\rm bj}M)^2]}{[k_{\rm T}^2 + x_{\rm bj}m_s^2 + (1 - x_{\rm bj})m_q^2 + x_{\rm bj}(x_{\rm bj} - 1)M^2]^2}. \quad (56)$$

These structure functions only depend on $x_{\rm bj}$ and $k_{\rm T}^2$ and are independent of Q^2, as would be anticipated for the parton model approximation. The equality $\mathcal{F}_1 = \mathcal{F}_2$ is a version of the Callan-Gross relation [41], but for the unintegrated structure functions. Note that the parton virtuality $\tilde{k}^2$ in Eq. (55) in the PDF is an approximation to the true parton virtuality.

To develop intuition about the approximations just made on the parton momentum, it is useful to Taylor expand the exact k^+, k^- and k^2 from Eqs. (18)–(21) through the first several powers of m^2/Q^2,

$$\xi = x_{\rm bj}\left[1 + \frac{k_{\rm T}^2 + m_q^2 - x_{\rm bj}^2M^2}{Q^2} - \frac{x_{\rm bj}^3M^2(k_T^2 + m_q^2) + x_{\rm bj}(k_T^2 + m_q^2)(k_T^2 + m_s^2 - M^2) - 2M^4x_{\rm bj}^4(x_{\rm bj} - 1)}{Q^4(x_{\rm bj} - 1)}\right] + O\left(\frac{m^6}{Q^6}\right), \quad (57)$$

$$k^- = -\frac{x_{\rm n}}{Q\sqrt{2}}\left[\frac{k_{\rm T}^2 + m_s^2 + (x_{\rm n} - 1)M^2}{1 - x_{\rm n}} - \frac{x_{\rm n}(k_{\rm T}^2 + m_q^2)(k_{\rm T}^2 + m_s^2)}{Q^2(x_{\rm n} - 1)^2}\right] + O\left(m \cdot \frac{m^5}{Q^5}\right), \quad (58)$$

$$k^2 = -\frac{k_{\rm T}^2 + x_{\rm n}[m_s^2 + (x_{\rm n} - 1)M^2]}{1 - x_{\rm n}} - \frac{x_{\rm n}(k_{\rm T}^2 + m_q^2)(k_{\rm T}^2 + [m_s + (x_{\rm n} - 1)M][m_s - (x_{\rm n} - 1)M])}{Q^2(x_{\rm n} - 1)^2} + O\left(m^2 \cdot \frac{m^4}{Q^4}\right). \quad (59)$$

Here we have expressed ξ in terms of $x_{\rm bj}$ because the leading power contribution to ξ is conventionally written as $x_{\rm bj}$. The lowest nonvanishing powers in Eqs. (58)–(59) match Eqs. (54)–(55), respectively, confirming that the approximations leading up to Eq. (56) are valid for sufficiently large Q. For k^- and k^2, it is more convenient to maintain expressions in terms of $x_{\rm n}$. Of course, $x_{\rm n}$ may be replaced everywhere here by $x_{\rm bj}$ without changing the validity of the expressions.

The formula for the $O(\lambda^2)$ PDF in Eq. (53) could also have been obtained directly from the operator definition of the collinear PDF, calculated in the scalar diquark field theory. The definition of the PDF emerges automatically from the constraints of factorization. This is an important aspect of the steps above, and is a key of factorization derivations.

V. EXACT AND FACTORIZED STRUCTURE FUNCTIONS: A COMPARISON

In this section we compare DIS structure functions in the exact calculation of Sec. III with the corresponding calculations in the factorization approximation of Sec. IV. We restrict consideration to unintegrated structure functions, differential in $k_{\rm T}$. This permits a direct examination of the impact of the approximations from the previous section point by point in transverse momentum. Exact kinematics involve sensitivity to all components of parton momentum, including parton virtuality, so the notion of factorization with a collinear PDF will not apply to the exact case. However, the terms in a direct m^2/Q^2 expansion of the exact result can hint at ways to correct the collinear picture.

The power counting in Eq. (34), with $m^2 \ll Q^2$, must be reasonably well satisfied for the steps of the previous section to constitute a good approximation. Namely, the magnitude of the quark virtuality $|k^2|$ must be small relative to the hard scale Q^2. While the distribution of k^2 in an isolated proton is an intrinsic property of the bound state, the range of k^2 probed in a DIS collision is sensitive to external kinematical parameters like $x_{\rm bj}$ and M. Therefore, the validity of the $|k^2| \ll Q^2$ assumption also depends on external kinematics.

To make this clear, one may directly examine the behavior of Eqs. (18)–(21) in various limiting cases. For example, consider fixed Q^2 and the limit of $x_n \to 1$. The $\pm$ components of k are then

$$k^+ \to \frac{Q}{\sqrt{2}}\left(1+\frac{m_q^2-m_s^2}{M^2+Q^2}\right)+O(|1-x_n|), \tag{60a}$$

$$k^- \to -\frac{1}{2\sqrt{2}Q}\left(Q^2-M^2+\frac{(M^2+Q^2)(2k_T^2+m_s^2+m_q^2)}{m_s^2-m_q^2}\right) + O(|1-x_n|). \tag{60b}$$

Next taking the large-Q^2 limit, the quark virtuality becomes

$$\lim_{m/Q\to 0}\lim_{x_n\to 1} k^2 = -\frac{Q^2}{2}\left(1+\frac{2k_T^2+m_q^2+m_s^2}{m_s^2-m_q^2}\right). \tag{61}$$

The typical value of $-k^2$ is therefore of order Q^2 in the simultaneous limits of large x_n and large Q. [From Eq. (59), this remains true if the order of the limits is reversed.] The increasing size of $|k^2|$ with increasing x_{bj} is a symptom of parton kinematics becoming noncollinear. As x_n becomes very large, it eventually becomes questionable whether an interpretation in terms of universal collinear parton densities is possible. We will return to this discussion in Sec. V D.

A. Values for m_q and m_s

To proceed with numerical calculations, we must return to the discussion in Sec. II B regarding choices for m_q and m_s. In QCD, the mass of the target remnant will tend to grow with energy and Q^2, so the choice of m_s requires greater care. Lower bounds on m_s can be obtained from elementary kinematic considerations. Since the invariant mass of the final state system cannot be less than that of the lowest baryon state, namely the nucleon, then

$$W^2(x_{bj},Q) = (p_s+p_q)^2 > M^2. \tag{62}$$

Working in the rest frame of the quark-diquark system,

$$M - m_q < m_s \le W(x_{bj},Q) - m_q. \tag{63}$$

This constrains m_s to lie in a band whose width depends on x_{bj} and Q, with the range decreasing as $x_{bj}\to 1$.

We are interested in the numerical effects of the factorization approximations for some selected fixed values of k^2. However, k^2 is determined by external kinematics and the field theory parameters m_q and m_s. Therefore, we will choose m_s on a case-by-case basis to ensure specific values of k^2 designed to test power counting assumptions for reasonable k^2. The relationship between k^2 and m_s depends on other kinematic parameters, so we will need to choose a new m_s for each kinematical scenario in order to keep k^2 fixed. To see this, note that for fixed x_{bj} and large Q^2, the relationship between m_s and k^2 is

$$m_s{}^2 \approx (1-x_{bj})\left(M^2+\frac{|k^2|}{x_{bj}}\right). \tag{64}$$

For different x_{bj}, m_s must be modified if k^2 is to remain fixed. In the next section we will use the exact relationship between m_q, m_s, k^2, and k_T to choose specific values for m_s and m_q so that $|k^2|$ is no greater than several hundred MeV at small k_T.

If the actual typical k_T, k^2, and m_q are clustered around a range of very small values, then collinear factorization might be satisfied with very high accuracy even for relatively small Q. However, phenomenological studies of transverse momentum dependence in semi-inclusive DIS restrict typical k_T widths to ≈500–800 MeV [36–38], while model-based estimates suggest $\langle k_T\rangle \approx 300$ MeV [21]. (See also Ref. [42] and references therein.) Thus, the values we choose for m_q and $|k^2|$ (or m_s) cannot be simultaneously much less than about 300 MeV without creating tension with measurements of transverse momentum dependence in semi-inclusive DIS. Also, Eq. (63) means that m_s cannot be much less than M if m_q is small. Therefore, we will choose combinations of m_s and m_q such that $|k^2|$ is several hundred MeV, m_q is in the vicinity of $m_q \approx 300$ MeV, and the peak of the transverse momentum distribution is not greater than 300 MeV. [This peak location is somewhat small relative to the above examples from phenomenology; this will ensure that we underestimate $O(k_T^2/Q^2)$ kinematical errors to the collinear factorization formula.] The details of the resulting example calculations are discussed in the following.

B. Which power corrections are most important?

In the canonical factorization approximations of Sec. IV, there are four independent types of neglected power-suppressed terms,

$$\sim\frac{m_q^2}{Q^2}; \quad \text{Type-A} \tag{65a}$$

$$\sim\frac{k^2}{Q^2}; \quad \text{Type-B} \tag{65b}$$

$$\sim\frac{k_T^2}{Q^2}; \quad \text{Type-C} \tag{65c}$$

$$\sim\frac{M^2}{Q^2}. \quad \text{Type-D} \tag{65d}$$

For the purposes of power counting, we use k^2 as the independent variable for Type-B corrections in place of m_s^2. Of course, beyond leading power-law corrections, these

suppression factors come in combinations. For example, the $\sim O(m^6/Q^6)$ power corrections include terms proportional to

$$\frac{k^2}{Q^2} \times \frac{k_T^2}{Q^2} \times \frac{M^2}{Q^2}. \tag{66}$$

Therefore, it is not generally meaningful to address Type-D suppressed corrections independently of Type-B and Type-C suppressed corrections. Effects from M^2/Q^2 in higher powers are sensitive to the range of k^2.

Still, it is possible in principle that corrections suppressed by exactly one type of factor in Eqs. (65a)–(65d) alone might be important. For example, it is reasonable to speculate that terms with *only* a Type-D suppression may be large, whereas terms with any of Type-A through Type-C suppressions are negligible. Now that the exact and factorized calculations of the structure functions in the quark-diquark theory are available to us, we can test the feasibility of such an approximation directly by examining the relative importance of Type-A through Type-C corrections as compared with pure Type-D corrections. When corrections from isolated M/Q terms are useful, the quality of the approximations from Sec. IV should nonetheless be nearly independent of the exact values of k_T, m_q and k^2, so long as they lie within a reasonable range. If, however, small variations in k_T, m_q or k^2 produce large changes in the quality of the factorization approximation, then target mass corrections from terms like Eq. (66) are too large to ignore, and it is unlikely that isolated M/Q corrections alone can improve accuracy.

To illustrate the numerical dependence of the structure functions on the mass parameters m_q and m_s, we show in Fig. 4 the unintegrated $\mathcal{F}_1(x_n, Q^2, k_T^2)$ structure function, weighted by k_T, as a function of k_T. (The results for the $\mathcal{F}_2$ structure function are qualitatively similar, and do not alter our conclusions.) We emphasize that these plots correspond to the k^- solution in Eq. (20b) for which $|k^2|$ may be small enough to yield parton model kinematics. The other solution is dealt with in the $O(\lambda^2)$ hard part. The kinematics are chosen to be representative of typical values relevant to large-x_{bj} studies at modern accelerator facilities, $x_{bj} = 0.6$ for $Q = 2$ GeV, which corresponds to $W \approx 2$ GeV, and a higher Q value, $Q = 20$ GeV, characteristic of the deep scaling region. For the quark mass we take $m_q = 0.3$ and 0.5 GeV, while the values for the diquark mass m_s are chosen to ensure that the quark virtuality $v \equiv \sqrt{-k^2} =$ 300 MeV or 500 MeV at $k_T = 0$. These values are chosen to be consistent with the kinematical constraints discussed in Sec. V A and, as seen in Fig. 4, they produce distributions peaked at k_T slightly less than ≈300 MeV. For the exact calculation, there is an integrable kinematical square root divergence at $k_T = k_{T\,max}$ that is an artifact of our simplification to a $2 \to 2$ process. All graphs from Fig. 2 are included now, as required for an $O(\lambda^2)$ treatment without kinematical approximations. Note that with exact kinematics it is now only the sum of the graphs in Fig. 2 that is gauge invariant.

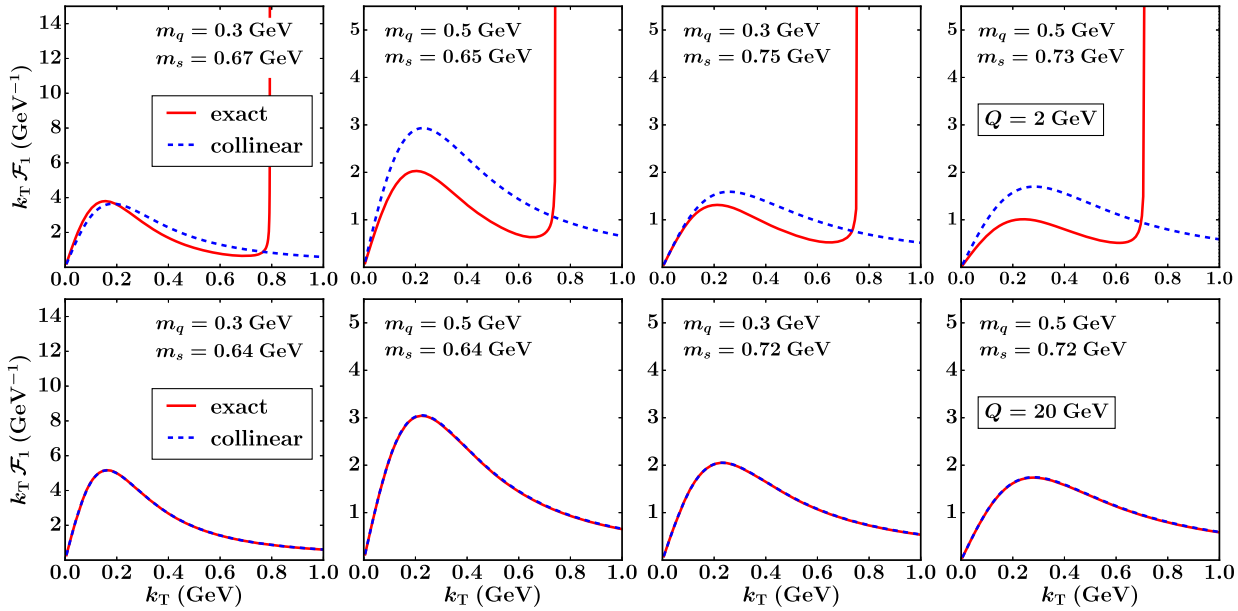

FIG. 4. The unintegrated structure function $k_T\mathcal{F}_1$ for $x_{bj} = 0.6$ and $Q = 2$ GeV (top row) and $Q = 20$ GeV (bottom row), for different values of m_q and m_s calculated using both the exact expressions (solid red curves) and the canonical collinear factorization approximation (dashed blue curves). The choices of m_s are to fix k^2 at the values discussed in Sec. V A. At the higher Q value the collinear calculation is almost indistinguishable from the exact, while at the lower Q value the exact calculation diverges as it approaches the kinematical upper limit of k_T.

At the higher Q value in Fig. 4 (bottom row), the factorized structure function is almost indistinguishable from the exact result. This validates that the approximate and exact calculations match in the large-Q limit, even for $k_T \gtrsim 1$ GeV. By contrast, for the lower Q value in Fig. 4 (top row), the exact calculation shows a clear deviation from the factorization approximation, both in size and shape. It is clear that if corrections of order ∼10% are important, then the roles of Type-A through Type-C corrections need to be considered on the same footing with Type-D corrections. The top row of Fig. 4 shows that the quality of the collinear factorization approximations for $Q\sim$ few GeV is indeed sensitive to the exact values of k^2 and m_q, whereas the applicability of the collinear factorization paradigm assumes independence of these nonperturbative parameters.

Even for the large Q value in Fig. 4, the shape of the k_T distribution is sensitive to the precise values of m_q and m_s, with the unintegrated structure function diverging for small values of k_T as m_q and $m_s \to 0$. This is to be expected because the k_T dependence near $k_T \approx 0$ is determined by the nonperturbative physics that regulates the infrared limit in the hadron wave function. More relevant is that the approximation errors are vanishingly small at $k_T < 1$ GeV and large Q, independently of m_s and m_q, as long as they lie within a reasonable range as discussed in Sec. V A.

Note also that the incoming quark virtuality k^2 is forced by kinematics to decrease to large negative values with increasing k_T. This is illustrated in Fig. 5, which shows the quark virtuality v as a function of k_T for fixed $x_{bj} = 0.6$ and $Q = 2$ and 20 GeV. The exact and approximate results for v coincide at the high Q value but differ visibly at small k_T and large k_T for the lower Q. At large k_T, the virtuality becomes linear with k_T, in accordance with Eq. (59) in the $m/Q \to 0$ limit. Even assuming $v < 1$ GeV for $k_T < 1$ GeV, the exact value of k^2 (and its dependence on k_T) impacts the shape of the k_T distribution and the quality of the usual factorization approximations.

C. The role of transverse momentum

The factorization approximations discussed in Sec. IV apply to the limit in which $k_T/Q \sim m/Q \ll 1$. In QCD, however, there are ultraviolet divergences from the integrals over transverse momentum in the PDF. The standard way to deal with this is to renormalize the PDF.

When Q is large, vertex corrections involve $O(Q^2)$ off-shell propagators, so the appropriate renormalization scale is $\mu \sim Q$. By comparison, the kinematics of real gluon emission restrict "large" transverse momentum to be $\lesssim O(Q\sqrt{1-x_{bj}}))$ [see Eq. (32)], so that the corresponding scale is $\mu \sim Q\sqrt{1-x_{bj}}$. (In our model calculation, the spectator plays the role kinematically of a real gluon emission.) If x_{bj} is not too large and $Q \gg m$, this mismatch between real and virtual emissions is not a serious problem because $k_{T\,max}$ is at least $O(Q)$ for all graphs. The collinear parton distribution Eq. (53) becomes, schematically,

$$f(x_{bj}) \propto \int_{M_{cut}^2}^{k_{T\,max}^2 \sim Q^2} \frac{dk_T^2}{k_T^2} \propto \ln\frac{Q^2}{m^2}, \tag{67}$$

where the lower bound M_{cut} on the integration is to restrict attention to the large $k_T \sim Q$ component of the integration [namely, the contribution to $f(x_{bj})$ from the large-k_T region varies logarithmically with Q^2]. As long as x_{bj} is not too large, Eq. (67) is consistent with the corresponding logarithms from virtual loops. The resulting $\log Q^2$ dependence is the familiar Q^2 dependence that arises in the standard DGLAP-type evolution equations which produce the logarithmic scaling violations of PDFs [43–45].

However, if $x_{bj} \approx 1 - m^2/Q^2$, then $k_{T\,max}$ is no greater than $O(m)$ and the large logarithms of Eq. (67) are no longer present. The ultraviolet divergences from loop integrals still need to be renormalized at the scale of the virtual photon ($\mu \sim Q$), so $\ln Q^2$ behavior from loop diagrams remain. This creates a mismatch between the

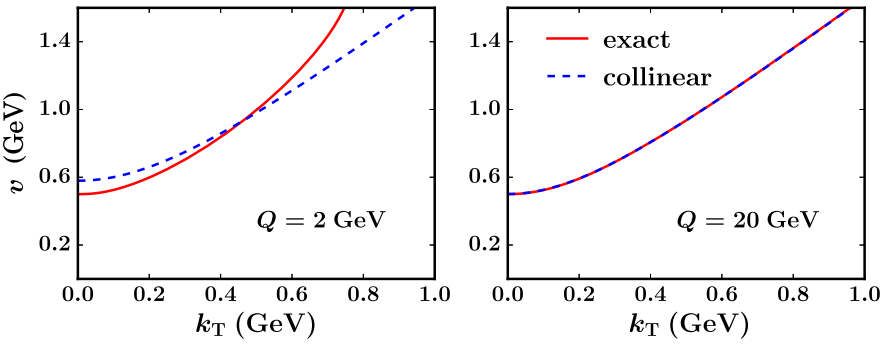

FIG. 5. The dependence of the parton virtuality $v \equiv \sqrt{-k^2}$ on k_T evaluated at exact (solid red curves) and approximate collinear (dashed blue curves) kinematics, for $x_{bj} = 0.6$ at fixed $Q = 2$ GeV (left panel) and $Q = 20$ GeV (right panel), for quark mass $m_q = 0.3$ GeV and spectator diquark mass m_s corresponding to $v(k_T = 0) = 0.5$ GeV (see Table I).

renormalization of real and virtual emissions. In QCD, the mismatch appears in high-order $\alpha_s(Q)$ contributions in the form of uncontrolled large finite parts, well-known as $\ln(1-x_{\rm bj})$ effects that, at a minimum, need to be resummed to all orders [14–17].

The small-$k_{\rm T\,max}$ problem is evident in the scalar diquark theory in Fig. 4 for the $x_{\rm bj}=0.6$ and $Q=2$ GeV kinematics. The value of $k_{\rm T}$ here approaches its kinematic upper bound at $k_{\rm T}\lesssim 1$ GeV, so the $k_{\rm T}\ll Q$ approximation begins to fail already for $k_{\rm T}\sim$ several hundred MeV. By contrast, for the higher Q value in Fig. 4, the kinematical upper bound on $k_{\rm T}$ lies well above 1 GeV (off the scale of the graphs). In QCD, this large-$k_{\rm T}$ region is generally describable by perturbative real gluon radiation.

To highlight the trends in $k_{\rm T}$ dependence at larger $x_{\rm bj}$ and moderate Q, it is useful to consider the exact $k_{\rm T\,max}$ from Eq. (32) in various limits. For example, in the limit of small m/Q with fixed $x_{\rm bj}$,

$$k_{\rm T\,max}=\frac{Q}{2}\left[\sqrt{\frac{1-x_{\rm bj}}{x_{\rm bj}}}-\sqrt{\frac{x_{\rm bj}}{1-x_{\rm bj}}}\frac{(2m_q^2+2m_s^2-M^2)}{2Q^2}+O\left(\frac{m^4}{Q^4}\left(\frac{x_{\rm bj}}{1-x_{\rm bj}}\right)^{3/2}\right)\right]. \tag{68}$$

This is the fixed-$x_{\rm bj}$ Bjorken limit applied to $k_{\rm T\,max}$, but a truncation of the series is liable to be a poor approximation to $k_{\rm T\,max}$ if $x_{\rm bj}$ is close to one. In that limit, it is more meaningful to Taylor expand first in powers of small $(1-x_{\rm bj})$ with fixed Q,

$$k_{\rm T\,max}=\frac{1}{2M}\sqrt{(m_q^2-M^2)^2+(m_s^2-m_q^2)^2+(m_s^2-M^2)^2-m_s^4-m_q^4-M^4}+O\left((1-x_{\rm bj})\frac{Q^3}{m^2}\right). \tag{69}$$

There is thus a finite and generally nonzero upper bound on $k_{\rm T}$ as $x_{\rm bj}$ becomes large. Indeed, if the collision is exactly elastic, $x_{\rm bj}\to 1$, and Eq. (10) requires $m_q+m_s=M$, which from Eq. (69) gives $k_{\rm T\,max}=0$.

To quantify errors in the integrations over $k_{\rm T}$, we define the integral over the exact structure function $\mathcal{F}_1$, for a fixed $x_{\rm bj}$ and Q, between $k_{\rm T}=0$ and the kinematic maximum, $k_{\rm T\,max}$,

$$I(x_{\rm bj},Q)\equiv\int_0^{k_{\rm T\,max}}{\rm d}k_{\rm T}k_{\rm T}\mathcal{F}_1^{\rm exact}(x_{\rm bj},Q,k_{\rm T}). \tag{70}$$

For the analogous calculation in the factorization approximation, on the other hand, there is no obvious upper bound on the $k_{\rm T}$ integration. In standard treatments, the upper limit, which we denote by $k_{\rm cut}$, need only be $O(Q)$, with the exact value otherwise arbitrary. Reasonable choices for $k_{\rm cut}$ could be $k_{\rm T\,max}$ or Q, for example. We define the integral over the structure function in the collinear approximation as

$$\hat{I}(x_{\rm bj},Q,k_{\rm cut})\equiv\int_0^{k_{\rm cut}}{\rm d}k_{\rm T}k_{\rm T}\mathcal{F}_1^{\rm approx}(x_{\rm bj},Q,k_{\rm T}). \tag{71}$$

In the limit of large Q, as long as $O(m)\ll k_{\rm cut}<O(Q)$, the factorization approximation should obey

$$\hat{I}(x_{\rm bj},Q,k_{\rm cut})\approx I(x_{\rm bj},Q). \tag{72}$$

In QCD, deviations from the equality of I and $\hat{I}$ are attributed to higher orders in $\alpha_s(Q)$. If, however, the ratio $I/\hat{I}$ deviates significantly from unity for a range of reasonable values for $k_{\rm cut}$, the validity of the collinear factorization approximation begins to become questionable. Also, $k_{\rm T\,max}$ needs to be $\gtrsim$1 GeV for gluon radiation effects to be perturbative. This is not the case for the $Q=2$ GeV results in Fig. 4.

In Table I we display the values for $I/\hat{I}$ using $k_{\rm cut}=k_{\rm T\,max}$ and $k_{\rm cut}=Q$ for the upper limit on the $k_{\rm T}$ integration in $\hat{I}$, for kinematics corresponding to Fig. 4, namely $x_{\rm bj}=0.6$ with $Q=2$ and 20 GeV. The values of m_q and m_s are also chosen to be as in Fig. 4, with $m_q=0.3$ or 0.5 GeV, and m_s computed by fixing the virtuality $v=0.3$ GeV (smaller m_s values, ∼0.64–0.67 GeV) or $v=0.5$ GeV (larger m_s values, ∼0.72–0.75 GeV) at $k_{\rm T}=0$. For the larger Q value, the results confirm that $I/\hat{I}$ is approximately unity for $k_{\rm cut}$ between $k_{\rm T\,max}$ and Q, independently of the exact values of m_q and m_s, so long as those values give reasonable $k_{\rm T}$ distributions that peak at ≈ a few hundred MeV. In contrast, for the smaller value of $Q=2$ GeV, the ratio $I/\hat{I}$ deviates significantly from unity, and has

TABLE I. Ratio of integrals $I/\hat{I}$ of exact to collinear $k_{\rm T}\mathcal{F}_1$ structure functions, where $I\equiv I(x_{\rm bj},Q)$ [Eq. (70)] and $\hat{I}\equiv\hat{I}(x_{\rm bj},Q,k_{\rm cut})$ [Eq. (71)], for different values of m_q and m_s as in Fig. 4, for $x_{\rm bj}=0.6$ and $Q=2$ and 20 GeV. The approximate collinear integral is evaluated for $k_{\rm cut}=Q$ and $k_{\rm cut}=k_{\rm T\,max}$.

	$Q=2$ GeV				$Q=20$ GeV			
m_q (GeV)	0.3	0.5	0.3	0.5	0.3	0.5	0.3	0.5
m_s (GeV)	0.67	0.65	0.75	0.73	0.64	0.64	0.72	0.72
$I/\hat{I}(k_{\rm T\,max})$	0.88	0.64	0.76	0.57	1.00	1.00	1.00	1.00
$I/\hat{I}(Q)$	0.67	0.45	0.49	0.35	0.90	0.88	0.86	0.85

stronger dependence on the exact value of $k_{\rm cut}$. Note that for $Q = 2$ GeV and $x_{\rm bj} = 0.6$, the maximum transverse momentum $k_{\rm T\,max} < 1$ GeV, so that the dependence on the $k_{\rm T}$ cutoff likely has its own nonperturbative contributions.

D. Purely kinematic target mass corrections

In the context of factorization derivations, the notion of purely kinematic target mass corrections is unambiguous. To see this, first return to the factorization approximations of Sec. IV, and assume that for a fixed $x_{\rm bj}$ and Q the ratio m^2/Q^2 is small enough that a power-law expansion exists and has reasonable convergence. The first few powers of the Taylor expansion of momentum components were displayed in Eqs. (57)–(59). Now assume that, beyond the lowest nonvanishing powers, the only non-negligible correction terms are those with powers of M/Q alone, while terms suppressed by higher powers of $k_{\rm T}/Q$, m_q/Q, or m_s/Q are small. Upon dropping these, Eqs. (57)–(59) become

$$\xi \to \xi_{\rm TMC} \equiv x_{\rm bj}\left[1 - \frac{x_{\rm bj}^2 M^2}{Q^2} + \frac{2M^4 x_{\rm bj}^4}{Q^4} + \cdots\right] = x_{\rm n}, \tag{73}$$

$$k^- \to k^-_{\rm TMC} \equiv -\frac{x_{\rm n}[k_{\rm T}^2 + m_s^2 + (x_{\rm n}-1)M^2]}{\sqrt{2}Q(1-x_{\rm n})}, \tag{74}$$

$$k^2 \to k^2_{\rm TMC} \equiv -\frac{k_{\rm T}^2 + x_{\rm n}[m_s^2 + (x_{\rm n}-1)M^2]}{1-x_{\rm n}}. \tag{75}$$

Comparing with Eqs. (54) and (55) confirms that using Eqs. (73)–(75) is identical to simply replacing $x_{\rm bj} \to x_{\rm n}$ in the standard collinear parton model approximation, Eq. (56). Indeed, the replacement of $x_{\rm n}$ by $x_{\rm bj}$ in Eq. (34) was unnecessary for deriving the factorization formula; the steps leading to the factorized hadronic tensor in Eq. (49) are equally valid if $x_{\rm bj}$ is replaced everywhere by $x_{\rm n}$.

There is, therefore, a natural meaning to purely kinematic TMCs: they are the terms that are kept in the factorization derivation when all components of external, physical momenta, such as Eqs. (3)–(4), are left unapproximated. Specifically, purely kinematical TMCs are those that arise from keeping the minus component of the target momentum P, which is normally approximated to zero, exact in Eq. (3). This automatically results in $x_{\rm n}$ scaling (often referred to in the literature as "ξ scaling", not to be confused with the ξ variable used for the "+" component of k here), as opposed to $x_{\rm bj}$ scaling.

Power corrections beyond those accounted for in Eqs. (73)–(75) are associated with $k_{\rm T}$, m_q, and k^2 dependence, and hence are unavoidably coupled to bound state dynamics that are both nonperturbative and noncollinear (for $k_{\rm T} \sim m$). For $x_{\rm bj} > 0.5$, some of the higher power corrections that only involve $k_{\rm T}$, m_q, and m_s are enhanced by powers of $x_{\rm bj}/(1-x_{\rm bj})$ relative to those that only contain M [see Eqs. (57)–(59) and Eq. (68)]. Moreover, the integration over $k_{\rm T}$ in QCD includes the full range of nonperturbative transverse momentum between 0 and ~1 GeV, and power corrections that depend on $k_{\rm T}$ can become quite large. By contrast, purely kinematical TMCs are suppressed at low $x_{\rm bj}$ by powers of $x_{\rm bj}^2 M^2/Q^2$. This suggests that purely kinematical TMCs alone are not likely to be sufficient in most interesting large-$x_{\rm bj}$ cases, except perhaps for unusually heavy hadrons. In other words, once Q is small enough (or $x_{\rm bj}$ large enough) for there to be sensitivity to purely kinematic TMCs, the effects of other types of power corrections, including noncollinear effects, already come into play.

To numerically compare purely kinematical TMCs with other power correction effects, we show the unintegrated structure $\mathcal{F}_1$ structure function for the exact calculation in Fig. 6, with $x_{\rm bj} = 0.6$ and $Q = 3$ GeV, and with the standard collinear approximation and with the collinear result corrected for target mass effects by rescaling $x_{\rm bj} \to x_{\rm n}$. Perhaps surprisingly, in this case the target mass corrected form deviates

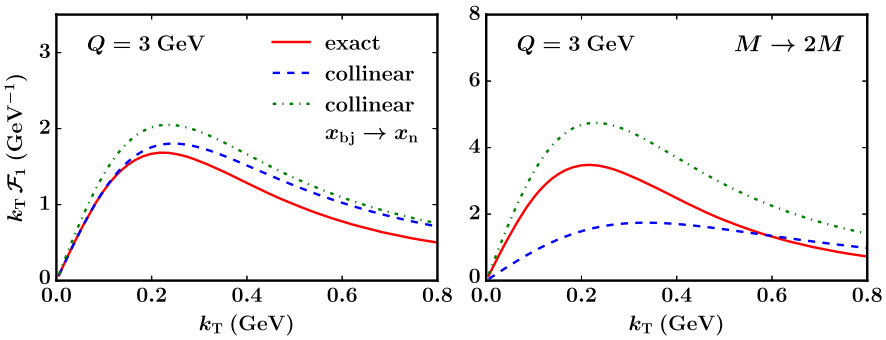

FIG. 6. Unintegrated structure function $k_{\rm T}\mathcal{F}_1$ for $x_{\rm bj} = 0.6$ and $Q = 3$ GeV, with quark mass $m_q = 0.3$ GeV and virtuality $v = 0.5$ GeV for the exact result (solid red curves), approximate collinear approximation (dashed blue curves), and collinear result with the replacement $x_{\rm bj} \to x_{\rm n}$ (dot-dashed green curves). The right-hand panel shows the results when the nucleon mass increased by a factor of 2.

further from the exact result than the uncorrected collinear approximation. The expectation that purely kinematic TMCs dominate if M is especially large is borne out in Fig. 6, where we compare the various calculations for the case when $M \to 2M$. Here, powers of M/Q are large and the expansion in powers of M/Q certainly fails. Thus, the $x_{\rm bj} \to x_{\rm n}$ replacement indeed improves the approximation, though there are still significant errors from the remaining neglected m/Q corrections that are not particularly small.

The phrase "purely kinematic TMCs" is sometimes used to characterize the $O(M^2/Q^2)$ correction terms first derived in the classic OPE analysis of Georgi and Politzer [21]. The results for the mass corrected structure functions in Ref. [21] [see Eqs. (4.19)–(4.22)] differ from those in Eqs. (73)–(75), in the form of additional corrections involving integrals over parton momentum fractions. These differences arise because Ref. [21] imposes the exact constraint $\tilde{k}^2 = 0$ for the quark momentum from the outset. As explained by Ellis *et al.* [18], the additional corrections in Ref. [21] originate from the integration over $k_{\rm T}$ when $\tilde{k}^2$ is held fixed at zero. In particular, Ref. [18] finds that the unintegrated structure function must have the functional form [see Eq. (1.22)]

$$\mathcal{F}_1 \sim \Phi\left(x_{\rm bj} + \frac{k_{\rm T}^2}{x_{\rm bj} M^2}\right) \theta(x_{\rm bj}(1 - x_{\rm bj})M^2 - k_{\rm T}^2). \quad (76)$$

(A similar analysis is given for polarized PDFs in Ref. [46].) Here, the $\tilde{k}^2 = 0$ condition constrains the behavior of the PDF to all orders in $x_{\rm bj} m_s^2/Q^2$, m_q^2/Q^2, and $k_{\rm T}^2/Q^2$. Furthermore, fixing $\tilde{k}^2 = 0$ removes the ultraviolet divergences in the integral over $k_{\rm T}$ that ultimately gives rise to the logarithmic behavior characteristic of the DGLAP evolution equations [43–45]. By contrast, factorization derivations impose no constraints on typical sizes for $\tilde{k}^2$ (recall Sec. IV) inside a PDF, instead leaving it to be determined by the intrinsic properties of the hadron.

The constraint $\tilde{k}^2 = 0$ in Eq. (76) is thus an extra dynamical assumption, and a rather restrictive one. This is illustrated, for example, by Fig. 5 and the discussions in Sec. V A. In field theory calculations of a PDF, k^2 tends to vary smoothly over a broad range between 0 and $O(-Q^2)$ (see Fig. 5), and indeed in an unregulated integration over $k_{\rm T}$, the virtuality $\tilde{k}^2$ diverges.

In practice, the $\tilde{k}^2 = 0$ constraint is rather difficult to achieve in field theories and realistic models, and it precludes order-by-order derivations of factorization. This can be understood by inspecting Eq. (53) and noting the distortions to the $O(\lambda^2)$ parton distribution that would be necessary to recover a form like Eq. (76).

Figures 4–6 emphasize that the structure functions are sensitive to the exact value of k^2, including $k^2 \neq 0$. At a minimum, the higher twist $k^2 \neq 0$ contributions in Ref. [18] are needed for consistent power counting. For the above reasons, we will restrict our use of the term "purely kinematical" TMCs to what is described in the context of Eqs. (73)–(75), namely, only the replacement $x_{\rm bj} \to x_{\rm n}$.

E. Help from large $\ln(1 - x_{\rm bj})$ resummation

Beyond leading power in Q^2, the integration of the large transverse momentum in Eq. (67) actually takes the form

$$\int_{M_{\rm cut}^2}^{k_{\rm T\,max}^2} \frac{{\rm d}k_{\rm T}^2}{k_{\rm T}^2} \propto \ln\left[\frac{Q^2}{M_{\rm cut}^2}\left(\frac{1 - x_{\rm bj}}{x_{\rm bj}} + \frac{(M^2 - 2m_q^2 - 2m_s^2)}{Q^2} + O\left(\frac{m^4}{Q^4}\frac{x_{\rm bj}}{1 - x_{\rm bj}}\right)\right)\right]$$
$$= \ln\frac{Q^2}{M_{\rm cut}^2} + \ln\left(\frac{1 - x_{\rm bj}}{x_{\rm bj}}\right) + \frac{x_{\rm bj}(M^2 - 2m_q^2 - 2m_s^2)}{(1 - x_{\rm bj})Q^2} + O\left(\frac{m^4}{Q^4}\frac{x_{\rm bj}^2}{(1 - x_{\rm bj})^2}\right). \quad (77)$$

In the region of $x_{\rm bj}$ where

$$\frac{x_{\rm bj} m^2}{Q^2} \ll 1 - x_{\rm bj} \ll 1, \quad (78)$$

the only non-negligible contributions in Eq. (77) are the terms $\ln Q^2$ and $\ln(1 - x_{\rm bj})$. The logarithms of $(1 - x_{\rm bj})$ appear at all orders in perturbation theory in collinear factorization, and much effort has been devoted to methods for resumming them in collinear perturbative QCD. It is important to remember, however, that the usefulness of such methods relies on the condition in Eq. (78) being fulfilled. If hadron mass corrections are large, for instance when $m^2/Q^2 \sim \alpha_s$, the expansion Eq. (77) may no longer be a useful approximation. In the literal limit $x_{\rm bj} \to 1$, it is impossible to fulfill Eq. (78).

There is of course no obvious sharp boundary between regions where perturbative $\ln(1 - x_{\rm bj})$ terms dominate and regions where $x_{\rm bj}$ is so large that power corrections dominate or the power expansion breaks down entirely and Eq. (78) fails. In principle, both the logarithmic and power correction effects are intertwined because they stem from the same underlying physical origin; the available phase space for final states becomes constricted as $x_{\rm bj} \to 1$, and the distinction between logarithmic effects and subleading power corrections becomes less clear-cut. For

example, it is equally valid to express the large logarithmic effects in Eq. (77) as $\ln(1-x_{\rm bj})$ or $\ln(1-x_{\rm n})$ simply by reorganizing power corrections accordingly. Thus, incorporating power corrections consistently in perturbative QCD may entail new techniques in addition to a merging of old ones.

An ideal formalism would smoothly connect a treatment that includes purely nonperturbative behavior at very large $x_{\rm bj}$ with resummation in the limit that the condition in Eq. (78) holds. This would be analogous to what occurs with TMD factorization, where a resummation of $\ln(q_{\rm T}^2/Q^2)$ holds when $m \ll q_{\rm T} \ll Q$, but nonperturbative intrinsic transverse momentum dependence contributes when $q_{\rm T}$ begins to approach m. It will be important to explore such effects in future work.

VI. SUMMARY

Let us conclude by returning to the goals listed at the end of Sec. I. If it is accepted that the range of values for m_q and m_s discussed in Secs. II B and V A is reasonable, then the results in Sec. V B indeed imply that all types of power corrections in Eqs. (65a)–(65b) are important in the range of $Q \sim 1$ GeV and $x_{\rm bj} \gtrsim 0.5$. For such kinematics, all components of partonic momentum are potentially nonnegligible, and a power series expansion around the collinear limit may not be sufficient. Here parton transverse momentum and parton virtuality are as important as the target mass in determining the size and behavior of power corrections to collinear factorization. Moreover, k^2 and $k_{\rm T}$ are generally not fixed, but rather are correlated with external kinematic variables such as $x_{\rm bj}$ and Q, and in principle take a spectrum of values in convolution integrals.

For slightly larger Q and smaller $x_{\rm bj}$, power corrections will be smaller but still possibly important. In all cases, they should be calculated explicitly in terms of higher-twist functions as in Ref. [18], or with generalizations of factorization that take parton kinematics more fully into account.

In the present work, we have placed our analysis of power corrections in the context of factorization derivations by first reviewing the canonical collinear factorization approximations for low-order graphs in Sec. IV. We view this as the appropriate approach to the treatment of power corrections because collinear factorization is, fundamentally, the first term in a $1/Q$ expansion, performed order by order in α_s in QCD, or in λ^2 in the scalar theory of Eq. (2).

There are opportunities for extending analyses like the one in Sec. V and perhaps using them directly for phenomenological modeling. In particular, it might be possible to improve constraints on numerical values for m_q and m_s in a model theory like the scalar Yukawa theory used here by determining if and how they can be connected to detailed considerations of nonperturbative physics in QCD. The values used in this paper were chosen through a combination of basic kinematical constraints, extractions of transverse momentum dependent functions, and mass scales typical of nonperturbative quark models. In the future, we hope to obtain tighter and more reliable estimates of the boundary to the factorization collinear regime by appealing to more sophisticated descriptions of nonperturbative physics. Including higher-order radiation to model the effects of parton showering may remove unrealistic features associated with having a fixed target remnant mass. Some of these considerations overlap with the discussions in Ref. [47] of the need to understand nonperturbative aspects of parton momentum.

We stress that there is, in principle, a distinction between the boundary of the collinear kinematics of collinear factorization and the boundary of the small-$\alpha_s(Q)$ perturbative regime more broadly. Thus, an exciting possibility is that there is a DIS regime at very large $x_{\rm bj}$ and large Q where collinear factorization kinematics break down entirely but an alternative small-$\alpha_s(Q)$ perturbative QCD method applies. An approach like that of Accardi and Qiu [48], which takes into account the role of final states in constraining overall kinematics, is likely needed, but in a form that incorporates more general noncollinear correlation functions. Generalizations of PDFs which smoothly map onto the elastic or exclusive limits may perhaps be appropriate to describe DIS at very large $x_{\rm bj}$. Models such as the quark-diquark theory used in this work can provide hints towards more optimal approaches. The concept of a virtuality-dependent function, discussed recently by Radyushkin [49,50], may also play an important role in an improved treatment. If a particular approximation is valid or useful, it should be possible to demonstrate the validity of the collinear approximation in the appropriate limits of Sec. IV. We plan to pursue this in future work.

ACKNOWLEDGMENTS

We thank A. Accardi, J. O. Gonzalez-Hernandez, S. Liuti, A. Radyushkin, and A. Rajan for useful discussions. We thank J. Collins for helpful comments on the text. This work was supported by the DOE Contract No. DE-AC05-06OR23177, under which Jefferson Science Associates, LLC operates Jefferson Lab. This material is based upon work supported by the U.S. Department of Energy, Office of Science, Office of Nuclear Physics, within the framework of the TMD Topical Collaboration.

APPENDIX: ELECTROMAGNETIC GAUGE INVARIANCE

In this appendix we explicitly demonstrate the electromagnetic gauge invariance of the hadronic tensor $W^{\mu\nu}$ for both the exact and approximate cases. Gauge invariance requires $q_\mu W^{\mu\nu} = 0$, where q_μ is the virtual photon momentum. In the case of the exact calculation in Eq. (18), this means

$$\sum_{j\in\text{graphs}} q_\mu \mathrm{T}_j^{\mu\nu}[\mathrm{Prop}]_j = 0, \tag{A1}$$

where j labels the diagrams in Fig. 2. To verify Eq. (A1), we first simplify the contraction for each diagram individually. For Fig. 2(a),

$$\begin{aligned} q_\mu \mathrm{T}_a^{\mu\nu}[\mathrm{Prop}]_a &= \frac{\mathrm{Tr}[(\not{P}+M)(\not{k}+m_q)\not{q}(\not{k}+\not{q}+m_q)\gamma^\nu(\not{k}+m_q)]}{(k^2-m_q^2)^2} \\ &= \frac{\mathrm{Tr}[(\not{P}+M)(\not{k}+m_q)(-(\not{k}-m_q)+\not{q}+\not{k}-m_q)(\not{k}+\not{q}+m_q)\gamma^\nu(\not{k}+m_q)]}{(k^2-m_q^2)^2} \\ &= \frac{-\mathrm{Tr}[(\not{P}+M)(\not{k}+\not{q}+m_q)\gamma^\nu(\not{k}+m_q)]}{(k^2-m_q^2)}. \end{aligned} \tag{A2a}$$

For the $1/Q$ suppressed contribution from Fig. 2(b),

$$\begin{aligned} q_\mu \mathrm{T}_b^{\mu\nu}[\mathrm{Prop}]_b &= \frac{\mathrm{Tr}[(\not{P}+M)\not{q}(\not{P}+\not{q}+M)(\not{k}+\not{q}+m_q)(\not{P}+\not{q}+M)\gamma^\nu]}{((P+q)^2-M^2)^2} \\ &= \frac{\mathrm{Tr}[(\not{P}+M)(-(\not{P}-M)+\not{q}+\not{P}-M)(\not{P}+\not{q}+M)(\not{k}+\not{q}+m_q)(\not{P}+\not{q}+M)\gamma^\nu]}{((P+q)^2-M^2)^2} \\ &= \frac{\mathrm{Tr}[(\not{P}+M)(\not{k}+\not{q}+m_q)(\not{P}+\not{q}+M)\gamma^\nu]}{((P+q)^2-M^2)}. \end{aligned} \tag{A2b}$$

The contribution to Eq. (A1) from the interference diagram Fig. 2(c) is

$$\begin{aligned} q_\mu \mathrm{T}_c^{\mu\nu}[\mathrm{Prop}]_c &= \frac{\mathrm{Tr}[(\not{P}+M)(\not{k}+m_q)\not{q}(\not{k}+\not{q}+m_q)(\not{P}+\not{q}+M)\gamma^\nu]}{(k^2-m_q^2)((P+q)^2-M^2)} \\ &= \frac{\mathrm{Tr}[(\not{P}+M)(\not{k}+m_q)(-(\not{k}-m_q)+\not{q}+\not{k}-m_q)(\not{k}+\not{q}+m_q)(\not{P}+\not{q}+M)\gamma^\nu]}{(k^2-m_q^2)((P+q)^2-M^2)} \\ &= \frac{\mathrm{Tr}[(\not{P}+M)(\not{k}+\not{q}+m_q)(\not{P}+\not{q}+M)\gamma^\nu]}{((P+q)^2-M^2)}, \end{aligned} \tag{A2c}$$

while contribution of the Hermitian conjugate of Fig. 2(c) is

$$\begin{aligned} q_\mu \mathrm{T}_d^{\mu\nu}[\mathrm{Prop}]_d &= \frac{\mathrm{Tr}[\not{q}(\not{P}+\not{q}+M)(\not{k}+\not{q}+m_q)\gamma^\nu(\not{k}+m_q)(\not{P}+M)]}{(k^2-m_q^2)((P+q)^2-M^2)} \\ &= \frac{\mathrm{Tr}[(-(\not{P}-M)+\not{q}+\not{P}-M)(\not{P}+\not{q}+M)(\not{k}+\not{q}+m_q)\gamma^\nu(\not{k}+m_q)(\not{P}+M)]}{(k^2-m_q^2)((P+q)^2-M^2)} \\ &= \frac{\mathrm{Tr}[(\not{k}+\not{q}+m_q)\gamma^\nu(\not{k}+m_q)(\not{P}+M)]}{(k^2-m_q^2)}. \end{aligned} \tag{A2d}$$

Thus,

$$q_\mu \mathrm{T}_a^{\mu\nu}[\mathrm{Prop}]_a + q_\mu \mathrm{T}_b^{\mu\nu}[\mathrm{Prop}]_b + q_\mu \mathrm{T}_c^{\mu\nu}[\mathrm{Prop}]_c + q_\mu \mathrm{T}_d^{\mu\nu}[\mathrm{Prop}]_d = 0. \tag{A3}$$

In the collinear approximation in Eq. (49), the hadronic tensor is gauge invariant if

$$q_\mu \mathrm{Tr}[H^\mu(Q^2)\hat{k}' H^{\dagger\nu}(Q^2)\hat{k}] = 0. \tag{A4}$$

This is easily verified as follows:

$$q_\mu \mathrm{Tr}[H^\mu(Q^2)\hat{k}' H^{+\nu}(Q^2)\hat{k}] = \mathrm{Tr}[\not{q}(\hat{k}+\not{q})\gamma^\nu \hat{k}] = 4((2\hat{k}\cdot q - Q^2)\hat{k}^\nu - \hat{k}^2 q^\nu)$$
$$= 4(2\hat{k}^+ q^- - Q^2)\hat{k}^+ = 4\left(2\frac{Q^2}{\sqrt{2}}\frac{Q^2}{\sqrt{2}} - Q^2\right)\frac{Q^2}{\sqrt{2}} = 0. \quad \text{(A5)}$$

Thus, electromagnetic gauge invariance is validated for both the exact and approximate, collinear cases.

[1] J. C. Collins, D. E. Soper, and G. Sterman, in *Perturbative Quantum Chromodynamics*, Advanced Series on Directions in High Energy Physics Vol. 5, edited by A. H. Mueller (World Scientific, Singapore, 1989), 1.
[2] P. Jimenez-Delgado, W. Melnitchouk, and J. F. Owens, J. Phys. G **40**, 093102 (2013).
[3] S. Forte and G. Watt, Annu. Rev. Nucl. Part. Sci. **63**, 291 (2013).
[4] J. Blümlein, Prog. Part. Nucl. Phys. **69**, 28 (2013).
[5] S. Bethke, G. Dissertori, and G. P. Salam, EPJ Web Conf. **120**, 07005 (2016).
[6] D. W. Duke and R. G. Roberts, Nucl. Phys. **B166**, 243 (1980).
[7] A. Devoto, D. W. Duke, J. F. Owens, and R. G. Roberts, Phys. Rev. D **27**, 508 (1983).
[8] E. D. Bloom and F. J. Gilman, Phys. Rev. D **4**, 2901 (1971).
[9] A. De Rújula, H. Georgi, and H. D. Politzer, Ann. Phys. (N.Y.) **103**, 315 (1977).
[10] E. C. Poggio, H. R. Quinn, and S. Weinberg, Phys. Rev. D **13**, 1958 (1976).
[11] X. Ji and P. Unrau, Phys. Rev. D **52**, 72 (1995).
[12] W. Melnitchouk, R. Ent, and C. Keppel, Phys. Rep. **406**, 127 (2005).
[13] A. Courtoy and S. Liuti, Phys. Lett. B **726**, 320 (2013).
[14] G. Sterman, Nucl. Phys. **B281**, 310 (1987).
[15] S. Catani and L. Trentadue, Nucl. Phys. **B327**, 323 (1989).
[16] Yu. L. Dokshitzer, G. Marchesini, and G. P. Salam, Phys. Lett. B **634**, 504 (2006).
[17] A. V. Manohar, Phys. Rev. D **68**, 114019 (2003).
[18] R. K. Ellis, W. Furmanski, and R. Petronzio, Nucl. Phys. **B212**, 29 (1983).
[19] R. L. Jaffe and M. Soldate, Phys. Rev. D **26**, 49 (1982).
[20] I. Schienbein *et al.*, J. Phys. G **35**, 053101 (2008).
[21] H. Georgi and H. D. Politzer, Phys. Rev. D **14**, 1829 (1976).
[22] O. Nachtmann, Nucl. Phys. **B63**, 237 (1973).
[23] K. G. Wilson, Phys. Rev. **179**, 1499 (1969).
[24] R. A. Brandt and G. Preparata, Nucl. Phys. **B27**, 541 (1971).
[25] N. H. Christ, B. Hasslacher, and A. H. Mueller, Phys. Rev. D **6**, 3543 (1972).
[26] S. Wandzura and F. Wilczek, Phys. Lett. **72B**, 195 (1977).
[27] J. Blümlein and A. Tkabladze, Nucl. Phys. **B553**, 427 (1999).
[28] A. De Rújula, H. Georgi, and H. D. Politzer, Phys. Rev. D **15**, 2495 (1977).
[29] D. J. Gross, S. B. Treiman, and F. A. Wilczek, Phys. Rev. D **15**, 2486 (1977).
[30] K. Bitar, P. W. Johnson, and W.-K. Tung, Phys. Lett. **83B**, 114 (1979).
[31] P. W. Johnson and W.-K. Tung, in *7th International Conference on Neutrinos, Weak Interactions and Cosmology—Neutrino '79, Bergen, Norway, 1979* (Fysisk Institutt, Bergen, 1979).
[32] F. M. Steffens, M. D. Brown, W. Melnitchouk, and S. Sanches, Phys. Rev. C **86**, 065208 (2012).
[33] S. B. Libby and G. Sterman, Phys. Rev. D **18**, 3252 (1978).
[34] T. Becher, A. Broggio, and A. Ferroglia, Lect. Notes Phys. **896**, 1 (2015).
[35] J. C. Collins, *Foundations of Perturbative QCD* (Cambridge University Press, Cambridge, England, 2011).
[36] R. P. Feynman, R. D. Field, and G. C. Fox, Phys. Rev. D **18**, 3320 (1978).
[37] M. Anselmino, M. Boglione, J. Gonzalez H., S. Melis, and A. Prokudin, J. High Energy Phys. 04 (2014) 005.
[38] A. Signori, A. Bacchetta, M. Radici, and G. Schnell, J. High Energy Phys. 11 (2013) 194.
[39] R. K. Bhaduri, *Models of the Nucleon: From Quarks to Soliton*, Lecture Notes and Supplements in Physics Vol. 22 (Addison-Wesley, Redwood City, 1988).
[40] A. Bacchetta, M. Diehl, K. Goeke, A. Metz, P. J. Mulders, and M. Schlegel, J. High Energy Phys. 02 (2007) 093; A. Radyushkin, arXiv:1702.01726 [hep-ph].
[41] C. G. Callan and D. J. Gross, Phys. Rev. Lett. **22**, 156 (1969).
[42] A. W. Thomas and W. Weise, *The Structure of the Nucleon* (Wiley-VCH, Berlin, 2001).
[43] V. N. Gribov and L. N. Lipatov, Sov. J. Nucl. Phys. **15**, 438 (1972).
[44] Y. L. Dokshitzer, Sov. Phys. JETP **46**, 641 (1977).
[45] G. Altarelli and G. Parisi, Nucl. Phys. **B126**, 298 (1977).
[46] U. D'Alesio, E. Leader, and F. Murgia, Phys. Rev. D **81**, 036010 (2010).
[47] M. Boglione, J. Collins, L. Gamberg, J. O. Gonzalez-Hernandez, T. C. Rogers, and N. Sato, Phys. Lett. B **766**, 245 (2017).
[48] A. Accardi and J. Qiu, J. High Energy Phys. 07 (2008) 090.
[49] A. Radyushkin, Phys. Lett. B **767**, 314 (2017).
[50] A. Radyushkin, Phys. Rev. D **95**, 056020 (2017).